Case study of the Bövik-Benveniste methodology for imperfect interface modeling of two-dimensional elasticity problems with thin layers

S. Baranova, S.G. Mogilevskaya*

Department of Civil, Environmental, and Geo-Engineering, University of Minnesota, Minneapolis, USA

Abstract

In this paper, a two-dimensional case study of the Bövik-Benveniste methodology for imperfect interface modeling of thin elastic layers is performed. The case study problem involves an infinite domain containing a coated circular-shaped fiber subjected to uniform loading at infinity. All phases of that composite system are assumed to be isotropic and linearly elastic. Using this case, the main assumptions of the methodology are analyzed, and a novel, complex variables-based approach for its implementation is developed. The proposed approach is used for derivations of the first, second, and third orders imperfect interface models for the case study problem. The models are tested for problems involving a wide range of governing parameters. It is demonstrated that the Bövik-Benveniste methodology allows for the construction of elastic interface models that behave satisfactorily at all ranges of layer stiffness.

Keywords: Imperfect interface modeling, Bövik-Benveniste methodology, high order models, complex variables-based approach

1. Introduction

Composite materials with thin coating layers and interfaces are encountered in a variety of engineering applications. Due to recent advances in surface engineering, it became possible to create thin films and coating layers whose surface-related properties are solely responsible for unique performance of new composites that is practically unachievable in bulk materials. Therefore, accurate modeling of thin layers is crucial for understanding intricate effects they produce in composite materials. This explains tremendous interest to the topic of interface modeling that resulted in large number of publications in which various models have been proposed and extensively studied in the context of heat conduction, elasticity,

Email address: mogil003@umn.edu (S.G. Mogilevskaya)

^{*}Corresponding author

thermoelasticity, etc., see comprehensive reviews in, e.g., Benveniste and Miloh (2001); Rubin and Benveniste (2004); Javili et al. (2013); Lebon and Rizzoni (2018); Dumont et al. (2016); Baranova et al. (2020); Serpilli et al. (2021); Firooz et al. (2021).

One approach in modeling thin layers, the so-called imperfect interface approach, consists in reducing a layer to a zero-thickness interface with jump conditions in relevant fields that are properly derived to mimic presence of the layer. As described in, e.g., Lebon and Rizzoni (2018); Baranova et al. (2020); Saeb et al. (2021), the imperfect interface models could be classified into two categories. The models of the first category are based on phenomenological considerations that endow an interface with its own energetic structure and require additional data (e.g., interface constitutive laws, material parameters, jump conditions across the interface, etc.) The models that belong to the second category are derived analytically from the fully resolved problem (that includes thin layer) using various types of asymptotic analyses.

In this work, we focus on the second category of imperfect interface models. In most publications, those models are derived using the following two approaches. First approach is based on the asymptotic expansion method in which the layer thickness is chosen as a small (perturbation) parameter. The early models obtained with this approach are reviewed in Klarbring (1991); Klarbring and Movchan (1998); Mishuris (2004); more recent reviews can be found in, e.g., Schmidt (2008); Lebon and Rizzoni (2011); Rizzoni and Lebon (2013); Rizzoni et al. (2014); Lebon and Rizzoni (2018); Serpilli et al. (2021). In this approach, the order of an interface model is defined by the highest power of perturbation parameter involved in the asymptotic series. Two different asymptotic techniques have been developed, one based on matched asymptotic expansions and the other one on variational formulation; their consistency and equivalence have been proved, in e.g., Rizzoni et al. (2014). The approach involves a recursive procedure to obtain higher terms of the asymptotic series and, in general, results into implicit forms of jump conditions across the interface.

The second approach is based on the use of Taylor series expansions of the fields involved. In such approach, the order of interface model is defined by the truncation order of Taylor series expansions. Significant contributions to the development of the latter approach are due to Hashin (Hashin, 2001, 2002), Bövik (Bövik and Olsson, 1992; Bövik, 1994), and Benveniste (Benveniste, 2006a,b). However, as explained in Benveniste (2006a), those researchers implemented the approach in two different ways. Hashin, see Hashin (2001, 2002), used one-step procedure in which the fields related to the layer material were expanded in the normal direction about the points located at the outer boundary of the layer and the expansions were used to evaluate the fields at the points located at its inner boundary. At both boundaries, the perfect bond conditions were enforced to exclude the fields related to the layer. The obtained jump conditions across the layer were treated as the jump conditions for the fields in two-phase imperfect interface model, in which the interface coincided with the trace of the inner boundary of the layer. The approach of Bövik and Benveniste (referred in the literature as the Bövik-Benveniste methodology) was first developed in Bövik and Olsson (1992); Bövik (1994) and further generalized in Benveniste (2006a,b). This approach is based on the following two-step procedure. At the first step, the fields at the points located at the mid-surface of the layer are expanded in the normal

direction about the points located at both boundaries and, after enforcing the perfect bond conditions, the jump conditions across the layer are obtained. At the second step, additional Taylor series expansions are used for the jumps of the first steps to eventually obtain the explicit expressions for the jump conditions across the interface, which coincides with the trace of the mid-surface. Later on, this methodology was used by several other authors, see, e.g., Zhu et al. (2011); Gu et al. (2011); Xu et al. (2016); Baranova et al. (2020); Kushch and Mogilevskaya (2021); Kushch (2021a,b). Unfortunately, despite clarifications provided in Benveniste (2006a), the distinctions between various one- and two-steps procedures were not always clearly made, sometimes confusing the jumps across the layer with those across the interface, see e.g. Lebon and Rizzoni (2018) for the description of the case when all phases in the three-phase configuration problem have the same properties. In the Bövik-Benveniste methodology, jumps across the layer (obtained at the first step) are, as expected, non-zero, while those across the zero-thickness interface (obtained at the second step) vanish. The solution of the two-phase configuration problem of a plane subjected to far-field load and prescribed vanishing jumps across the interface is analytical and it coincides with that for the problem of a homogeneous plane subjected to the same far-field load. Thus, the fields at the traces of the layer boundaries are exactly evaluated, and the subtraction of the fields associated with one boundary from those associated with the other produces exact jump conditions across the layer in the three-phase configuration problem. In other words, the procedure of finding jumps across the layer in three-phase configuration problems with the Bövik-Benveniste methodology requires an additional post-processing step consisting in the evaluation of the fields at the traces of the layer boundaries after solving the two-phase configuration problems.

The Bövik-Benveniste methodology was successfully used in potential problems, see Benveniste (2006b); Baranova et al. (2020), where the interface models of arbitrary orders were constructed for interfaces of arbitrary smooth curvatures and wide range of problem parameters. However, there was an issue with its applications in elasticity problems containing very stiff layers. The issue was identified by Benveniste and Berdichevsky (2010) who reported that "the numerical results for the $O(h^2)$ version ... revealed a serious deficiency consisting in the fact that for very stiff interphases its predictions do not improve over the corresponding results of its O(h) version ... and even fall more distant from the exact solution", and concluded that "the construction of an $O(h^2)$ version ... in elasticity which behaves satisfactorily at all ranges of interphase stiffness remains an open issue."

The main goal of this paper is to resolve this issue and demonstrate, using the case study problem of an infinite coated fiber of circular cross-section, that the Bövik-Benveniste methodology can be successfully implemented in elastic problems with wide ranges of problem parameters. To achieve this goal, we perform detailed study of the methodology main assumptions, develop novel complex variables-based implementation of the methodology, and formulate, for the first time, third order interface model for the case study problem.

The paper is structured as follows. In Section 2, we formulate the case study problem. In Section 3, we review theoretical tools that are used in subsequent sections and reformulate the problem in terms of complex variables. In Section 4 (with the details provided in Appendix A), we discuss the Bövik-Benveniste methodology and validate its underlining as-

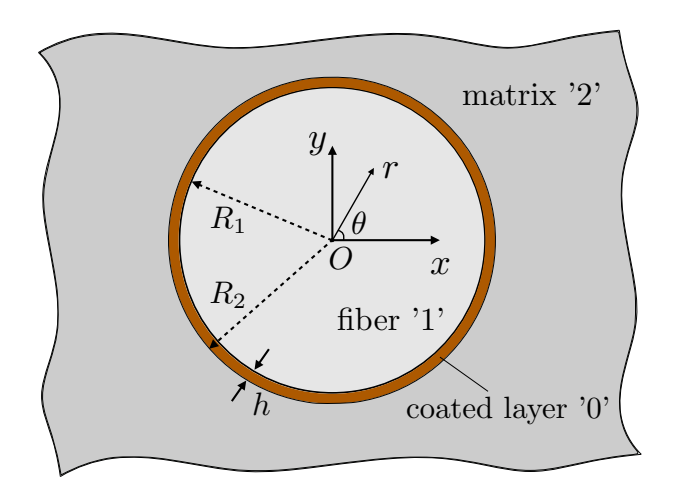


Figure 1: Case study problem: coated fiber of circular cross-section embedded in an infinite matrix

sumptions for the problem under study. In Section 5 (with the details provided in Appendix B), we develop novel, complex variables-based, implementation of the Bövik-Benveniste methodology for the problem and derive jump conditions for the imperfect interface models of first, second, and third orders. In Section 6, we use those models to obtain solutions of the case study problem for wide range of governing parameters and far-field loadings. Finally, in Section 7, we draw conclusions and discuss directions of future work.

2. Problem formulation for the case study

Consider a two-dimensional linear elastic plane strain problem involving an infinite matrix subjected to uniform far-field load and containing a coated fiber of circular cross-section (Fig. 1). Assume that media of the fiber, the coating layer, and the matrix (referred as medium '1', '0', and '2', respectively) are isotropic and characterized by the shear module $\mu^{(p)}$ and Poisson's ratios $\nu^{(p)}$, where $p = \{0, 1, 2\}$. Also, consider the polar coordinate system (r, θ) and assume that its center is chosen to be located at the center of the fiber. The inner and outer radii of the coating layer are denoted as R_1 and R_2 , respectively. Thus, the layer's thickness is constant and equal to $h = R_2 - R_1$.

The following boundary conditions of perfect contact are imposed:

$$\begin{cases}
\mathbf{u}^{(0)}/_{r=R_q} = \mathbf{u}^{(q)}/_{r=R_q}, \\
\mathbf{T}^{(0)}/_{r=R_q} = \mathbf{T}^{(q)}/_{r=R_q},
\end{cases} \qquad q = \{1, 2\}, \tag{1}$$

where $\boldsymbol{u}^{(p)}$ and $\boldsymbol{T}^{(p)} = \boldsymbol{\sigma}^{(p)} \cdot \boldsymbol{n}_q$ are respectively the displacement and traction vectors in the corresponding medium 'p', $\boldsymbol{\sigma}^{(p)}$ is the stress tensor in the medium 'p', and \boldsymbol{n}_q is the unit vector normal to the corresponding boundary of the layer $r = R_q$. The notation $\cdot/_{r=R_q}$ identifies the limit value of a corresponding field at the layer boundary described by $r = R_q$.

3. Preliminaries: concise review of relevant aspects

In our study of Bövik-Benveniste methodology, we will use several tools of the complex variables theory. Thus, we start with the review of relevant concepts of that theory, introduce basic notations, and reformulate the case study problem in terms of complex variables.

3.1. Holomorphic functions

The complex variable z can be expressed via the local coordinates as $z = re^{i\theta}$, where i refers to the imaginary unit defined by $i^2 = -1$. Below, we will use the following standard definition of the derivative of the complex-valued function f(z) at some point a belonging to an open set Ω in which f(z) is defined:

$$\frac{\mathrm{d}f(z)}{\mathrm{d}z}\bigg|_{z=a} = \lim_{z \to a} \frac{f(z) - f(a)}{z - a}.$$
 (2)

For this derivative to exist, its value should not depend on the way in which z approaches a. The complex-valued function for which complex derivatives exist at any point of Ω is called *holomorphic*.

The existence of complex derivative (2) is guaranteed if the real and imaginary parts of the function f(z) = u(x, y) + iv(x, y) satisfy the so-called Cauchy-Riemann conditions. Those conditions can be formulated in the polar coordinates as

$$u_{,r} = \frac{1}{r}v_{,\theta}, \qquad v_{,r} = -\frac{1}{r}u_{,\theta}$$
 (3)

or in more concise form as

$$f_{,r} = -\frac{i}{r}f_{,\theta},\tag{4}$$

where notations $(\cdot)_{,r}$ and $(\cdot)_{,\theta}$ referred to partial derivatives of corresponding function with respect to r and θ .

It can be seen from equation (4) that, for holomorfic function, its derivative with respect to r can always be transferred to that with respect to θ . This fact is essential for the developments of our approach.

Another essential fact is that conditions (3) ensure existence of the derivative $d^n f(z)/dz^n$ of arbitrary order n (Ahlfors, 1979; Shabat, 1976). Thus, holomorphic functions are infinitely differentiable functions.

The complex derivative of the holomorphic function f(z) can be expressed in terms of polar coordinates as

$$\frac{\mathrm{d}f(z)}{\mathrm{d}z} = \frac{e^{-i\theta}}{2} \left(f_{,r} - \frac{i}{r} f_{,\theta} \right). \tag{5}$$

Taking into account Cauchy-Riemann conditions (4), Eq.(5) leads to

$$\frac{\mathrm{d}f(z)}{\mathrm{d}z} = -\frac{ie^{-i\theta}}{r}f_{,\theta}.\tag{6}$$

Thus, all derivatives of holomorphic functions can be expressed via those with respect to θ . For example, the expressions for the second and third order derivatives of the holomorphic function with respect to r can be obtained with the use of Eq. (4) as

$$f_{,rr} = \left(-\frac{i}{r}f_{,\theta}\right)_{,r} = \frac{1}{r^2}\left(if_{,\theta} - f_{,\theta\theta}\right),$$

$$f_{,rrr} = \left[\frac{1}{r^2}\left(if_{,\theta} - f_{,\theta\theta}\right)\right]_{,r} = \frac{1}{r^3}\left(-2if_{,\theta} + 3f_{,\theta\theta} + if_{,\theta\theta\theta}\right).$$
(7)

3.1.1. Case problem formulation in terms of complex variables

Let us reformulate the case problem in terms of complex variables. For that, we introduce the complex displacement and complex traction at the point z as

$$u(z) = u_x + iu_y,$$

$$\sigma(z) = \sigma_n + i\sigma_s,$$
(8)

where u_x and u_y are the displacement components in the global Cartesian coordinates of (Fig. 1) and σ_n and σ_s are the normal and shear traction components in the local coordinates.

Additionally, we introduce the resultant force f(z) as

$$f'(z) = \sigma(z), \tag{9}$$

where the symbol $(\cdot)'$ identifies the complex derivative $d(\cdot)/dz$.

The perfect bound boundary conditions could be reformulated in terms of complex variables fields as

$$\begin{cases} u^{(0)}/_{|z|=R_q} = u^{(q)}/_{|z|=R_q}, \\ \sigma^{(0)}/_{|z|=R_q} = \sigma^{(q)}/_{|z|=R_q}, \end{cases} q = \{1, 2\},$$
(10)

where notation |z| refers to the absolute value (modulus) of complex variable z and it is equal to r.

Sometimes, it might be convenient to reformulate the second condition of Eqs. (10) in terms of the resultant force f as

$$f^{(0)}/_{|z|=R_q} = f^{(q)}/_{|z|=R_q}.$$
 (11)

To complete the complex variables formulation for the case problem, we introduce the following combinations for the stress components of the uniform far-field load:

$$\sigma_1^{\infty} = \sigma_{xx}^{\infty} + \sigma_{yy}^{\infty},
\sigma_2^{\infty} = \sigma_{yy}^{\infty} - \sigma_{xx}^{\infty} - 2i\sigma_{xy}^{\infty},$$
(12)

where σ_{xx}^{∞} , σ_{yy}^{∞} , and σ_{xy}^{∞} are prescribed far-field stress tensor components.

3.1.2. Kolosov-Muskhelishvili potentials

The complex variables representations for the displacements and tractions of two-dimensional elasticity are given by the following Kolosov-Muskhelishvili formulae (Muskhelishvili, 1963):

$$2\mu u(z) = \kappa \varphi(z) - z\overline{\varphi'(z)} - \overline{\psi(z)},$$

$$\sigma(z) = \varphi'(z) + \overline{\varphi'(z)} + \frac{\mathrm{d}\overline{z}}{\mathrm{d}z} \left(z\overline{\varphi''(z)} + \overline{\psi'(z)} \right).$$
(13)

where the parameter κ is defined as $\kappa = 3 - 4\nu$ in plane strain and $\kappa = (3 - \nu)/(1 + \nu)$ in plain stress, a bar over a symbol denotes complex conjugation, and $\varphi(z)$ and $\psi(z)$ are the so-called Kolosov-Muskhelishvili potentials. Those potentials are holomorphic functions meaning that they are infinitely differentiable over z and equal, locally, to their complex Taylor series.

The complex variables representation for the resultant force f(z) is

$$f(z) = \varphi(z) + z\overline{\varphi'(z)} + \overline{\psi(z)}. \tag{14}$$

With the use of Eqs. (13) and (14), the potentials $\varphi(z)$ and $\psi(z)$ can be expressed via the complex displacement and resultant force as

$$\varphi = \frac{1}{\kappa + 1} (2\mu u + f),$$

$$\psi = \frac{1}{\kappa + 1} \left[\kappa \overline{f} - 2\mu \overline{u} - \overline{z} (2\mu u' + f') \right].$$
(15)

Additionally, far-field conditions can re-formulated via the potentials as

$$\varphi^{\infty}(z) = \frac{\mu^{(p)} \left(\kappa^{(2)} + 1\right) \sigma_1^{\infty} z}{\mu^{(2)} \left(\kappa^{(p)} + 1\right) \frac{\sigma_1^{\infty} z}{4}},$$

$$\psi^{\infty}(z) = \frac{\mu^{(p)} \left(\kappa^{(2)} + 1\right) \overline{\sigma}_2^{\infty} z}{\mu^{(2)} \left(\kappa^{(p)} + 1\right) \frac{\overline{\sigma}_2^{\infty} z}{2}},$$
(16)

where p = 1 if $|z| \le R_1$, p = 0 if $R_1 < |z| \le R_2$, and p = 2 if $|z| \ge R_2$.

4. Discussion of the Bövik-Benveniste methodology

In this section, we discuss the basic steps of the Bövik-Benveniste methodology and its main assumptions.

This methodology (Bövik and Olsson, 1992; Benveniste, 2006b) consists of two steps:

1. In the first step, using Taylor series expansions for the relevant fields inside the layer, jump conditions in those fields across the layer are obtained in such a way that the fields related to medium '0' are eliminated due to the use of perfect bond conditions. The resulting jump conditions contain the fields related to media '1' and '2' only.

2. In the second step, the two-phase configuration is considered in which the phases are separated by the interface, typically chosen to coincide with the mid-line of the layer. Then, it is required that the jumps in the relevant fields across the traces of layer's boundaries remain to be the same as the corresponding jumps obtained in the first step. Finally, Taylor series expansions are used in such a way that the fields involving in the jump conditions of the first step are let to approach the interface from both sides, resulting in the final jump conditions across the interface.

This methodology implies two major assumptions.

The first assumption requires the fields be differentiable up to a desired order, which allows for the use of truncated Taylor series up to that order. In our complex variable-based approach, this requirement is fulfilled by using Kolosov-Muskhelishvili formulae of Eq. (13) and truncated series expansions of involved infinitely differentiable holomorphic functions.

The second assumption implies that the original three-phase configuration problem can be reduced to the two-phase configuration one, if the medium between the corresponding boundary of the layer and the interface (a curve inside the layer) is replaced with the medium (that of a fiber or a matrix) in which the trace of corresponding layer's boundary is located. This effectively means that the medium of the fiber (medium '1') and that of the matrix (medium '2') are expanded up to the interface, thus, eliminating the layer (medium '0'). After such procedure, the jumps in the relevant fields across the traces of layer's boundaries must be the same as the corresponding jumps in the original problem.

This assumption that, in general, is not trivial is correct for the case study problem. From the analytical solution for three-phase configuration problem reviewed in Appendix A, it can be seen that the expressions for the displacements and tractions at the layer boundaries have the forms of complex Fourier series with only few nonzero coefficients. The solutions of the two-phase configuration problems could be obtained by using either complex integral equations in which the boundary unknowns are approximated by complex Fourier series, e.g., Mogilevskaya and Crouch (2002); Mogilevskaya et al. (2008); Zemlyanova and Mogilevskaya (2018), or complex series expansions for the potentials involved (Taylor series for the fiber and Laurent series for the matrix), see, e.g., Ru (1999); Sudak and Mioduchowski (2002) and the references therein. In both cases, it can be shown that the displacements and tractions at the traces of the layer boundaries can also be expressed in the forms of complex Fourier series. The unknown coefficients involved in the approximations for the two-phase configuration problem can be exactly found from the solution of the linear algebraic system obtained by equating the analytical expressions for the jumps of the original problem and the orthogonality property of complex Fourier series.

However, the Bövik-Benveniste methodology (as all other imperfect interface approaches) is based on the use of series expansions in terms of layer's thickness h. The truncation order of the series determines the order of interface model.

Below we check how many terms in the truncated series of such kind are needed to accurately compute solutions for the jumps in two-phase configuration, using the corresponding analytical solutions for three-phase configuration.

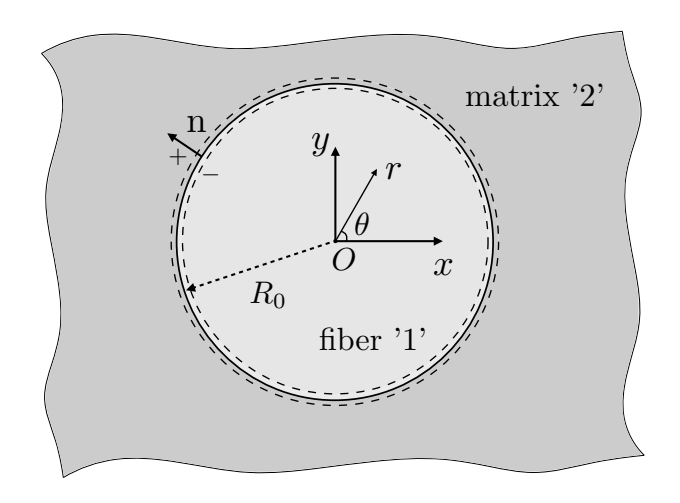


Figure 2: Two-phase configuration problem: a fiber and an infinite matrix separated by a circular interface of radius R_0

4.1. Approximations of the jumps across the traces of layer's boundary in two-phase configuration using analytical solution for three-phase configuration

Consider two-phase configuration problem of Fig. 2 that includes the fiber (medium '1') and the matrix (medium '2') separated by a zero-thickness interface, which here is chosen to be a circle of radius $R_0 = (R_1 + R_2)/2$.

The complex displacements $u^{(1)}(z)$ and $u^{(2)}(z)$ at the points $z_q = R_q e^{i\theta}$, $q = \{1, 2\}$ can be expressed in terms of Taylor series expansions about the point $z_0 = R_0 e^{i\theta}$, as

$$u^{(1)}(z)|_{z=z_1} = u^{(1)}(z)/_{z=z_0} + \sum_{n=1}^{\infty} \frac{(R_1 - R_0)^n}{n!} \frac{\partial^n u^{(1)}(z)}{\partial r^n} /_{z=z_0},$$
(17)

$$u^{(2)}(z)|_{z=z_2} = u^{(2)}(z)/_{z=z_0} + \sum_{n=1}^{\infty} \frac{(R_2 - R_0)^n}{n!} \frac{\partial^n u^{(2)}(z)}{\partial r^n} /_{z=z_0}.$$
 (18)

By subtracting Eq. (17) from Eq. (18) and using the fact that $R_1 - R_0 = -h/2$ and $R_2 - R_0 = h/2$, the jump in complex displacement across the layer can be obtained as

$$u^{(2)}(z)|_{z=z_{2}} - u^{(1)}(z)|_{z=z_{1}} = u^{(2)}(z)/_{z=z_{0}} - u^{(1)}(z)/_{z=z_{0}} + \sum_{n=1}^{\infty} \frac{1}{n!} \left(\frac{h}{2}\right)^{n} \left[\frac{\partial^{n} u^{(2)}(z)}{\partial r^{n}} \middle/_{z=z_{0}} - (-1)^{n} \frac{\partial^{n} u^{(1)}(z)}{\partial r^{n}} \middle/_{z=z_{0}} \right].$$

$$(19)$$

Similarly, the jump in complex traction from $|z| = R_2$ to $|z| = R_1$ can be expressed as

$$\sigma^{(2)}(z)|_{z=z_{2}} - \sigma^{(1)}(z)|_{z=z_{1}} = \sigma^{(2)}(z)/_{z=z_{0}} - \sigma^{(1)}(z)/_{z=z_{0}} + \sum_{n=1}^{\infty} \frac{1}{n!} \left(\frac{h}{2}\right)^{n} \left[\frac{\partial^{n} \sigma^{(2)}(z)}{\partial r^{n}} \middle/_{z=z_{0}} - (-1)^{n} \frac{\partial^{n} \sigma^{(1)}(z)}{\partial r^{n}} \middle/_{z=z_{0}} \right].$$
(20)

We then make use of analytical solution for the three-phase configuration problem of Appendix A in order to obtain closed-form expressions for the jumps in the fields across the layer (from $|z| = R_2$ to $|z| = R_1$).

To demonstrate that the jumps of Eqs. (19), (20) can reproduce with any desirable degree of accuracy those analytical solutions, we use the fact that, for the case of uniform far-field load, various solutions for the two-phase configuration problems are available. Those are e.g., the displacement representations of Christensen and Lo (1979); Christensen (2012), for the simple shear far-field load (rewritten in a slightly different form in Mogilevskaya et al. (2019)), or well-known representations for hydrostatic far-field load (also reviewed in Mogilevskaya et al. (2019)). With the use of such representations and standard superposition, expressions for more general cases of uniform far-field loads can be obtained.

The representations of that kind (that involve unknown coefficients) and their traction counterparts can be substituted into the right-hand sides of Eqs. (19), (20), while the left-hand sides of those equations can be evaluated using the analytical solutions for the corresponding three-phase configuration problems. Naturally, in this process, infinite series involved in the equations have to be truncated up to a certain order N, that leads to the error of $O(h^{N+1})$. Such procedure leads to the system of linear algebraic equations in terms of the unknown coefficients.

To illustrate the procedure, consider the simple shear loading case ($\sigma_{xx}^{\infty} = -\sigma_{yy}^{\infty} = \sigma_{d}^{\infty}$, $\sigma_{xy}^{\infty} = 0$), for which the representations for the normal and tangential displacement components are (Christensen and Lo, 1979)

• inside the fiber

$$u_r^{(1)}(z) = \frac{R_0}{4\mu^{(1)}} \left[d_1 \frac{r}{R_0} + \left(\kappa^{(1)} - 3\right) a_1 \frac{r^3}{R_0^3} \right] \cos 2\theta,$$

$$u_\theta^{(1)} = \frac{R_0}{4\mu^{(1)}} \left[-d_1 \frac{r}{R_0} + \left(\kappa^{(1)} + 3\right) a_1 \frac{r^3}{R_0^3} \right] \sin 2\theta;$$
(21)

• inside the matrix

$$u_r^{(2)} = \frac{R_0}{4\mu^{(2)}} \left[2\sigma_d^{\infty} \frac{r}{R_0} + \left(\kappa^{(2)} + 1\right) a_3 \frac{R_0}{r} + c_3 \frac{R_0^3}{r^3} \right] \cos 2\theta,$$

$$u_\theta^{(2)} = \frac{R_0}{4\mu^{(2)}} \left[-2\sigma_d^{\infty} \frac{r}{R_0} - \left(\kappa^{(2)} - 1\right) a_3 \frac{R_0}{r} + c_3 \frac{R_0^3}{r^3} \right] \sin 2\theta,$$
(22)

in which a_1, d_1, a_3 , and c_3 are unknown coefficients. The components $u_r^{(q)}$ and $u_{\theta}^{(q)}$ are related to the complex displacement as

$$u_r^{(q)} + iu_\theta^{(q)} = e^{-i\theta}u^{(q)}(z). \tag{23}$$

The use of Eqs. (21)-(22) together with the plane strain relations between stresses, strains, and displacements, leads to the following expressions for the normal and tangential traction components:

• inside the fiber

$$\sigma_r^{(1)} = \frac{1}{2} d_1 \cos 2\theta,$$

$$\sigma_\theta^{(1)} = \frac{1}{2} \left(-d_1 + \frac{6a_1 r^2}{R_0^2} \right) \sin 2\theta;$$
(24)

• inside the matrix

$$\sigma_r^{(2)} = \frac{1}{2} \left(2\sigma_d^{\infty} - 4a_3 \frac{R_0^2}{r^2} - 3c_3 \frac{R_0^4}{r^4} \right) \cos 2\theta,$$

$$\sigma_{\theta}^{(2)} = -\frac{1}{2} \left(2\sigma_d^{\infty} + 2a_3 \frac{R_0^2}{r^2} + 3c_3 \frac{R_0^4}{r^4} \right) \sin 2\theta.$$
(25)

The coefficients a_1 , d_1 , a_3 , and c_3 are found from the linear system that is formulated as explained above, i.e. using Eqs. (19) and (20), in which the analytical solutions of Appendix A are used in the left-hand sides, while representations (21)-(25) are used in the right-hand sides.

The resulting linear system can be rewritten in the matrix form as

$$AX = Y, (26)$$

where $X = [a_1, d_1, a_3, c_3]^T$ is the vector of the unknown coefficients, superscript "T" refers to transposition, $Y = [Y_1, Y_2, Y_3, Y_4]^T$ with

$$Y_{1} = A_{-12} - A_{-11} - \frac{R_{2}\sigma_{d}^{\infty}}{2\mu^{(2)}};$$

$$Y_{2} = A_{32} - A_{31};$$

$$Y_{3} = -B_{-22} + B_{-21} + \sigma_{d}^{\infty};$$

$$Y_{4} = -B_{22} + B_{21},$$

$$(27)$$

in witch A_{-11} , A_{-12} , A_{31} , A_{32} , B_{-21} , B_{-22} , B_{21} , and B_{22} are the governing coefficients for the analytical solution of three-phase configuration (given in Appendix A.1), and A is the 4×4 matrix

$$A = \begin{bmatrix} 3R_0b_{23}/4\mu^{(1)} & -R_1/4\mu^{(1)} & \kappa^{(2)}R_0b_{10}/4\mu^{(2)} & 0\\ -\kappa^{(1)}R_0b_{23}/4\mu^{(1)} & 0 & R_0b_{10}/4\mu^{(2)} & R_0b_{12}/4\mu^{(2)}\\ -3b_{22}/2 & 1/2 & b_{11}/2 & 0\\ 3b_{22}/2 & 0 & 3b_{11}/2 & 3b_{13}/2 \end{bmatrix},$$
(28)

in which

$$b_{1j} = 1 + \sum_{n=1}^{N} (-1)^n \left(\frac{h}{2R_0}\right)^n \frac{(n+j)!}{j!n!},$$

$$b_{2j} = 1 + \sum_{n=1}^{J} (-1)^n \left(\frac{h}{2R_0}\right)^n \frac{j!}{n!(j-n)!},$$
(29)

and J is defined as

$$J = \min(j, N) = \begin{cases} j, & N \ge j, \\ N, & N < j. \end{cases}$$
(30)

We start testing the above procedure using trivial case of homogeneous medium. In such case, the stresses inside the system are uniform and equal to those due to the simple shear far-field load, while the displacements vary linearly. This case corresponds to the three-phase configuration problem with $\mu^{(p)} = \mu$ and $\nu^{(p)} = \nu$ for $p = \{0, 1, 2\}$. Analytical solution of Appendix A provides the following expressions for the governing coefficients

$$B_{-21} = B_{-22} = \sigma_d^{\infty}, \quad B_{21} = B_{22} = 0,$$

 $A_{-11} = R_1 \sigma_d^{\infty} / 2\mu, \quad A_{-11} = R_2 \sigma_d^{\infty} / 2\mu, \quad A_{31} = A_{31} = 0.$ (31)

The use of (31) in linear system (26) leads, for any N, to the following closed-form solutions:

$$d_1 = 2\sigma_d^{\infty}, \quad a_1 = a_3 = c_3 = 0.$$
 (32)

It is clear from equations (21)-(22), (24)-(25), and (32) that the fields inside all constituents of two-phase configuration are indeed the same as those in homogeneous medium.

We will now proceed with the testing of the procedure using three examples that involve layers of different thicknesses and elastic properties. We will demonstrate that, by appropriately choosing value of N for each case, we can accurately simulate the jump conditions across the layer in three-phase configuration. For all three examples, we choose the same ratio $\mu^{(1)}/\mu^{(2)} = 5$ and take the values of Poisson's ratios to be $\nu^{(p)} = 0.35$ ($p = \{0, 1, 2\}$). The dimensionless far-field simple shear load is $\sigma_d^{\infty}/\mu^{(2)} = 1$, which might not be realistic but chosen here and below for convenience.

As the first example, we consider the case of thin and soft layer characterized by the dimensionless shear modulus $\mu^{(0)}/\mu^{(2)} = 1.3 \cdot 10^{-5}$ and dimensionless thickness $\varepsilon = h/R_0 = 0.001$. By choosing values of $N = \{1, 2, 3\}$, we solved corresponding systems of equations (26) and evaluated the displacement and traction jumps across the traces of the layer boundary in two-phase configuration. Figure 3 presents the normalized jumps in normal and tangential displacement components as well as the normalized jumps in the corresponding traction components. The following notations are adopted:

$$[(\cdot)] = (\cdot)^{(2)}\Big|_{r=R_2} - (\cdot)^{(1)}\Big|_{r=R_1}. \tag{33}$$

Additionally, Fig. 3 plots absolute errors of the corresponding solutions defined as

$$E_{u_r} = \frac{1}{R_0} | \llbracket u_r \rrbracket_{\text{approx}} - \llbracket u_r \rrbracket_{\text{exact}} |,$$

$$E_{u_\theta} = \frac{1}{R_0} | \llbracket u_\theta \rrbracket_{\text{approx}} - \llbracket u_\theta \rrbracket_{\text{exact}} |,$$

$$E_{\sigma_r} = \frac{1}{\mu^{(2)}} | \llbracket \sigma_r \rrbracket_{\text{approx}} - \llbracket \sigma_r \rrbracket_{\text{exact}} |,$$

$$E_{\sigma_\theta} = \frac{1}{\mu^{(2)}} | \llbracket \sigma_\theta \rrbracket_{\text{approx}} - \llbracket \sigma_\theta \rrbracket_{\text{exact}} |,$$
(34)

where subscripts "approx" and "exact" identify approximate solutions of two-phase configuration (obtained by solving linear system (26)) and exact solution of three-phase configuration (obtained analytically), respectively.

For this example, the values of the exact solutions for the normalized jumps $[u_r/R_0]$ and $[u_\theta/R_0]$ are of order 1 and those for $[\sigma_r/\mu^{(2)}]$ and $[\sigma_\theta/\mu^{(2)}]$ are of orders 10^{-7} and 10^{-4} , respectively. As it can be seen from Fig. 3, the approximate solutions for the normalized jumps in displacement components are sufficiently accurate even for N=1, with E_{u_r} and E_{u_θ} being relatively small (less than $8 \cdot 10^{-7}$) with respect to the orders of corresponding exact solutions. For the normalized jumps in traction components, approximate solutions are sufficiently accurate starting only with N=2, with E_{σ_r} and E_{σ_θ} being less than $7 \cdot 10^{-9}$.

In the second example, we consider thin and stiff layer characterized by the dimensionless shear modulus $\mu^{(0)}/\mu^{(2)}=1.3\cdot 10^{10}$ and dimensionless thickness $\varepsilon=0.001$. For this example, the exact solutions for the normalized jumps $[u_r/R_0]$ and $[u_\theta/R_0]$ are given by very small values (they are of order 10^{-12} and 10^{-5} , respectively), while those of $[\sigma_r/\mu^{(2)}]$ and $[\sigma_\theta/\mu^{(2)}]$ are of order 1. Figure 4 presents normalized jumps in normal and tangential displacement and traction components and corresponding absolute errors. It can be seen that the approximate solutions for the jumps in traction components are sufficiently accurate starting with N=1 with E_{σ_r} and E_{σ_θ} being less than $4\cdot 10^{-6}$. The approximate solutions for the jumps in tangential displacement are sufficiently accurate starting only from N=2, with E_{u_θ} being less than $4\cdot 10^{-10}$. The approximate solution for the normalized jump in normal displacement is sufficiently accurate only for N=4 with E_{u_r} being less than $3\cdot 10^{-16}$ that exceeds machine accuracy.

In the third example, we consider stiff and relatively thick layer with dimensionless shear modulus $\mu^{(0)}/\mu^{(2)} = 1.3 \cdot 10^5$ and dimensionless thickness $\varepsilon = 0.1$. The exact solutions for this example are defined by very small values of the normalized jumps $[u_r/R_0]$ and $[u_\theta/R_0]$ (of order 10^{-7} and 10^{-3} , respectively) and by values of normalized $[\sigma_r/\mu^{(2)}]$ and $[\sigma_\theta/\mu^{(2)}]$ that are of order 1. The normalized jumps in normal and tangential displacement and traction components and corresponding absolute errors for this example are plotted on Fig. 5. The approximated solutions for the normalized jumps in traction components are sufficiently accurate starting with N=1, with E_{σ_r} and E_{σ_θ} being less than $5 \cdot 10^{-2}$. The approximate solution for the normalized jump in tangential displacement is sufficiently accurate approximate solution for the normalized jump in normal displacement is achieved only from N=6, with E_{u_r} being less than 10^{-8} .

Similarly to the examples described above for simple shear far-field load, we considered examples (involving wide variety of governing parameters) for much simpler case of hydrostatic load. As in the three examples considered above, it was concluded that the analytical solutions for the jumps across the layer could always be accurately represented by the approximate solutions for the corresponding two-phase configuration problems, if appropriate values of N are chosen.

In the above developments, we benefited from the existence of analytical solution for the three-phase configuration problem. While the right-hand sides of Eqs. (19) and (20) are series expansions in terms of parameter h, the left-hand sides of those equations involve

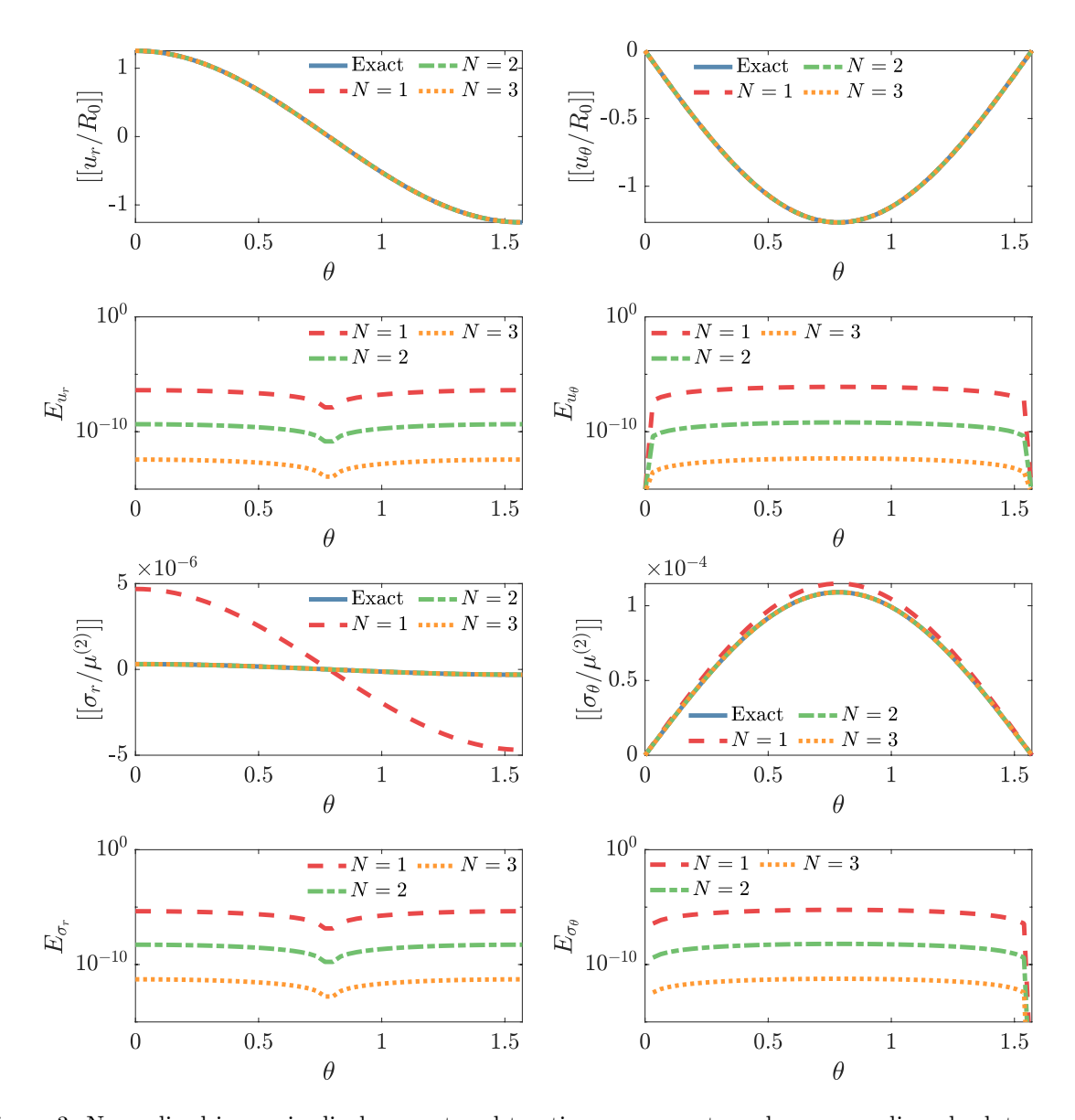


Figure 3: Normalized jumps in displacement and traction components and corresponding absolute errors plotted with respect to θ . Problem-specific parameters are $\sigma_d^\infty/\mu^{(2)}=1$, $\mu^{(1)}/\mu^{(2)}=5$, $\mu^{(0)}/\mu^{(2)}=1.3\cdot 10^{-5}$, and $\varepsilon=0.001$. (For interpretation of the references to colour in this figure legend, the reader is referred to the Web version of this article.)

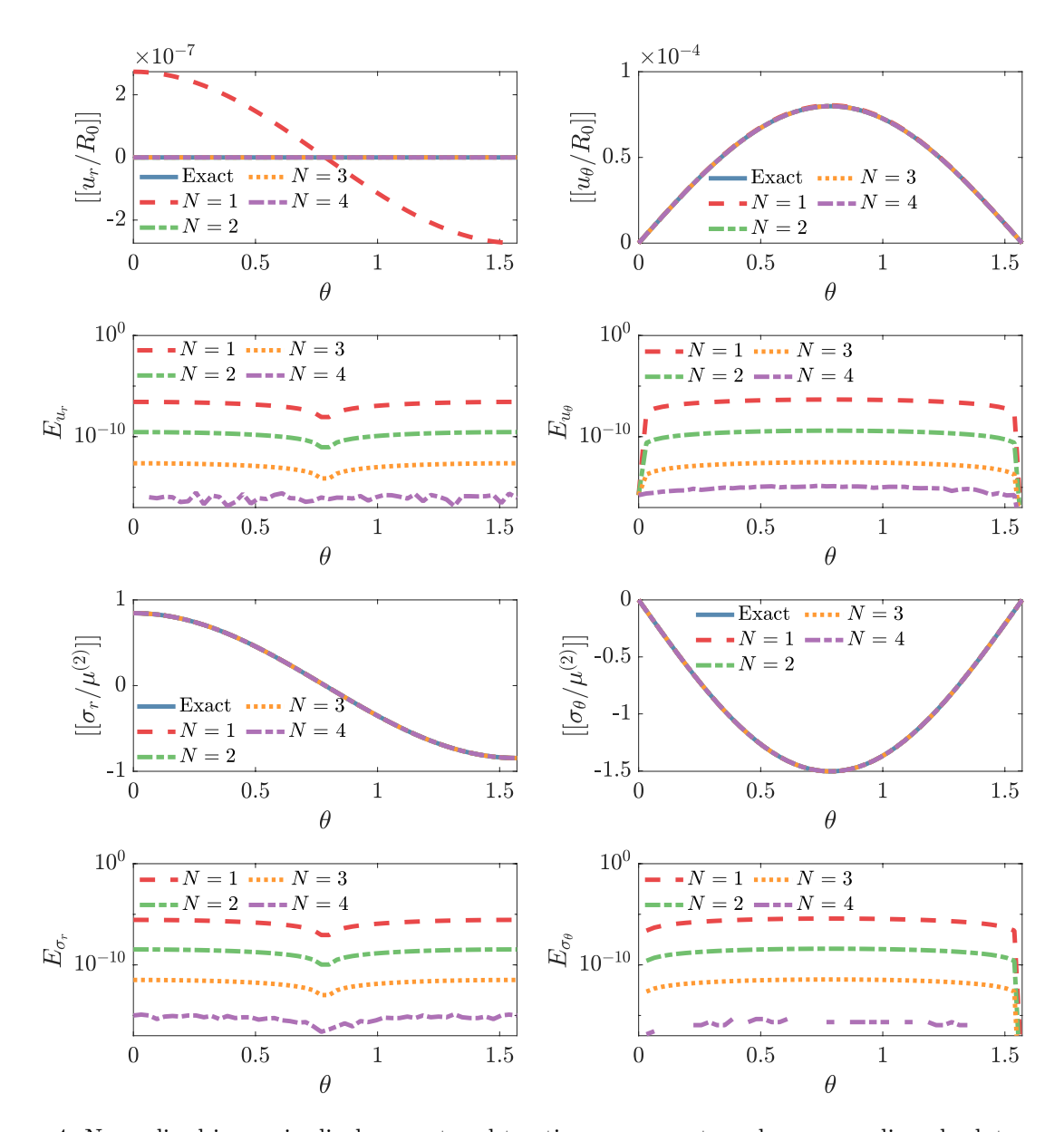


Figure 4: Normalized jumps in displacement and traction components and corresponding absolute errors plotted with respect to θ . Problem-specific parameters are $\sigma_d^\infty/\mu^{(2)}=1$, $\mu^{(1)}/\mu^{(2)}=5$, $\mu^{(0)}/\mu^{(2)}=1.3\cdot 10^{10}$, and $\varepsilon=0.001$. (For interpretation of the references to colour in this figure legend, the reader is referred to the Web version of this article.)

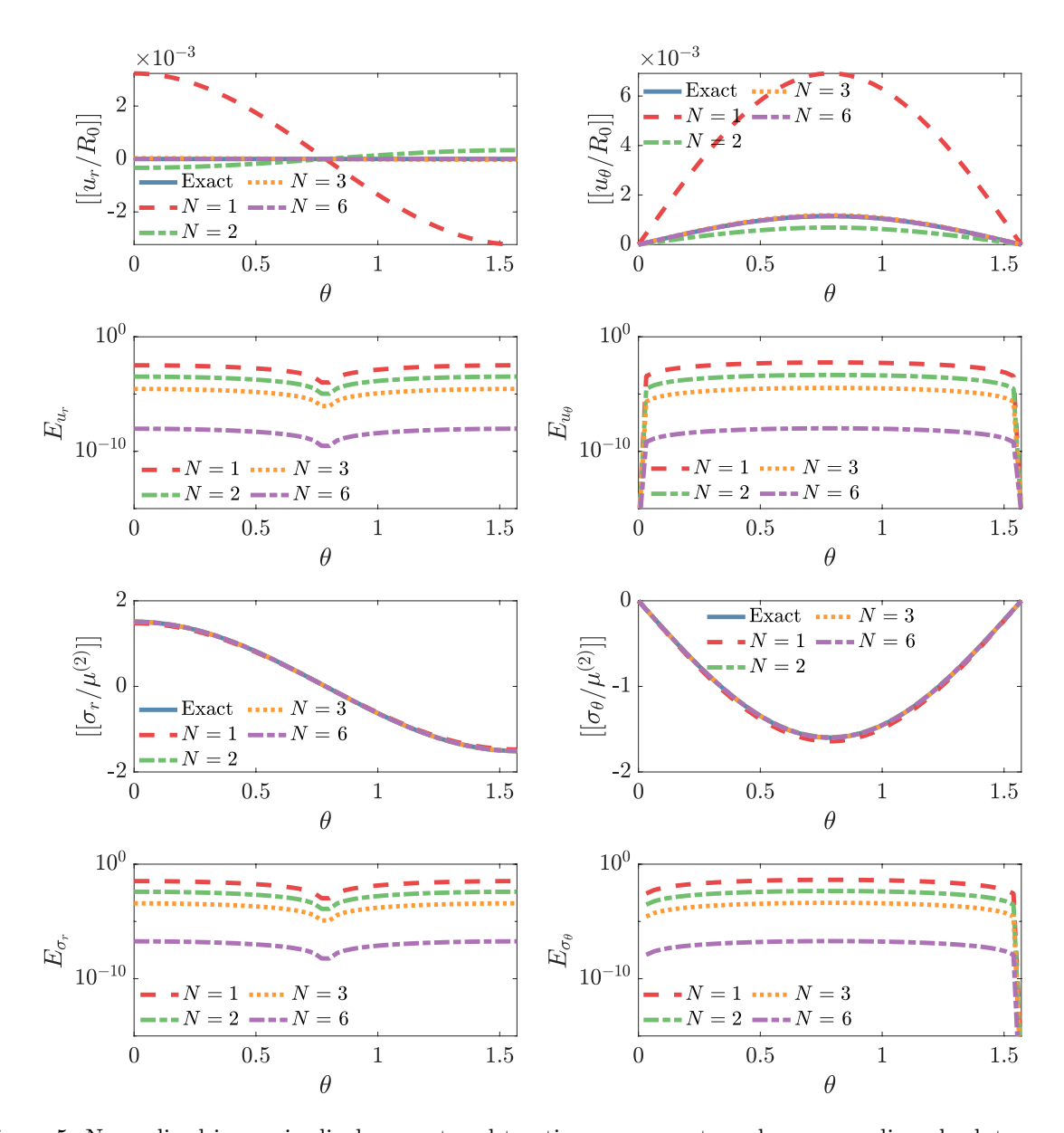


Figure 5: Normalized jumps in displacement and traction components and corresponding absolute errors plotted with respect to θ . Problem-specific parameters are $\sigma_d^\infty/\mu^{(2)}=1$, $\mu^{(1)}/\mu^{(2)}=5$, $\mu^{(0)}/\mu^{(2)}=1.3\cdot 10^5$, and $\varepsilon=0.1$. (For interpretation of the references to colour in this figure legend, the reader is referred to the Web version of this article.)

analytical solutions with the coefficients that include the parameters $\beta = R_1^2/R_2^2$ and β^{-1} , which themselves could be sums of some infinite series in terms of h, see, e.g., Eq. (A.11). In fact, the right-hand sides of Eqs. (19) and (20) represent exact series expansions of the corresponding analytical solutions in terms of h; it is not straightforward to obtain such expansions from the analytical solutions themselves.

In the Bövik-Benveniste methodology, analytical solutions are not employed (those are not usually available). Rather the jumps across the layer in the original problem are approximated by the truncated series expansions in terms of h; the truncation order defines the order of a specific model. Thus, it should be expected that the approximate solutions obtained by following the steps of that methodology would have slower convergence rates than those described in this section. It will be shown in the next sections, that the low order models do not work well for the cases of very stiff layers.

5. Complex variables-based implementation of the Bövik-Benveniste methodology

In this section, we describe complex variables-based implementation of the Bövik-Benveniste methodology without using any prior information on the solution of the three-phase configuration problem. First, we proceed with deriving the first order imperfect interface model. Next, we list relevant jump conditions for the second and third order models.

5.1. Derivation of the first order interface model

Consider complex variables formulation of case study problem of Section 3.1.1. For the sake of brevity, we introduce new notation $\varphi_q^{(p)}$ as a limit value of $\varphi^{(p)}$ when the latter approaches $z = z_q$ $(q = \{1, 2\})$ from corresponding medium "p" $(p = \{0, 1, 2\})$. Similar notations will be used for all fields considered thereafter. The limit values of derivatives of those fields will be denoted as, e.g., $(\varphi_{\theta}^{(p)})_q$.

Next, using Eqs. (13)-(15), Eq. (6), boundary conditions (10), and new notations, we reformulate the boundary conditions via the Kolosov-Muskhelishvili potentials $\varphi^{(p)}(z)$ and $\psi^{(p)}(z)$ (p=0,1,2) of Section 3.1.2, as

$$\varphi_{q}^{(0)} = \frac{1}{\kappa^{(0)} + 1} \left\{ a^{(q)} \varphi_{q}^{(q)} - b^{(q)} \left[i e^{2i\theta} \overline{\left(\varphi_{,\theta}^{(q)} \right)_{q}} + \overline{\psi_{q}^{(q)}} \right] \right\},
\psi_{q}^{(0)} = \frac{1}{\kappa^{(0)} + 1} \left\{ c^{(q)} \overline{\varphi_{q}^{(q)}} + b^{(q)} \left[2i \overline{\left(\varphi_{,\theta}^{(q)} \right)_{q}} + \overline{\left(\varphi_{,\theta\theta}^{(q)} \right)_{q}} \right] + d^{(q)} \psi_{q}^{(q)} \right.
\left. + i e^{-2i\theta} \left[\left(a^{(q)} - d^{(q)} \right) \left(\varphi_{,\theta}^{(q)} \right)_{q} - b^{(q)} \overline{\left(\psi_{,\theta}^{(q)} \right)_{q}} \right] \right\},$$
(35)

where

$$a^{(q)} = \frac{\mu^{(0)}}{\mu^{(q)}} \kappa^{(q)} + 1, \qquad b^{(q)} = \frac{\mu^{(0)}}{\mu^{(q)}} - 1,$$

$$c^{(q)} = \kappa^{(0)} - \kappa^{(q)} \frac{\mu^{(0)}}{\mu^{(q)}}, \qquad d^{(q)} = \kappa^{(0)} + \frac{\mu^{(0)}}{\mu^{(q)}}.$$
(36)

Now we perform the two steps procedure of the Bövik-Benveniste methodology, using complex variables.

First step: Jump conditions across the layer

We start from expanding potential $\varphi^{(0)}$ at $z_0 = R_0 e^{i\theta}$ in terms of Taylor series expansions about the two points $z_q = R_q e^{i\theta}$ (q = 1, 2) in the normal direction as

$$\varphi^{(0)}(z_0) = \varphi_q^{(0)} + \sum_{n=1}^{\infty} \frac{(R_0 - R_q)^n}{n!} \left(\frac{\partial^n \varphi^{(0)}}{\partial r^n}\right)_q.$$
 (37)

Next, we truncate expansions (37) up to the first order as

$$\varphi^{(0)}(z_0) = \varphi_q^{(0)} + (R_0 - R_q) \left(\varphi_{,r}^{(0)}\right)_q + O(h^2). \tag{38}$$

Using Cauchy-Riemann conditions (4) and the fact that

$$R_q = R_0 + (-1)^q \frac{h}{2} \tag{39}$$

we get

$$\varphi^{(0)}(z_0) = \varphi_q^{(0)} + (-1)^q \frac{ih}{2R_q} \left(\varphi_{,\theta}^{(0)}\right)_q + O(h^2). \tag{40}$$

Then, we subtract the value of $\varphi^{(0)}(z_0)$ given by Eq. (40) for q=2 from that for q=1 and obtain

$$\varphi_2^{(0)} - \varphi_1^{(0)} = -\frac{ih}{2} \left[\frac{1}{R_1} \left(\varphi_{,\theta}^{(0)} \right)_1 + \frac{1}{R_2} \left(\varphi_{,\theta}^{(0)} \right)_2 \right] + O(h^2). \tag{41}$$

Finally, using boundary condition (35), we obtain the following jump condition across the layer:

$$\sum_{q=1}^{2} (-1)^{q} \left\{ a^{(q)} \varphi_{q}^{(q)} - b^{(q)} \left[i e^{2i\theta} \overline{\left(\varphi_{,\theta}^{(q)} \right)_{q}} + \overline{\psi_{q}^{(q)}} \right] \right\}$$

$$= -\frac{ih}{2} \sum_{q=1}^{2} \frac{1}{R_{q}} \left\{ a^{(q)} \left(\varphi_{,\theta}^{(q)} \right)_{q} + b^{(q)} e^{2i\theta} \left[2 \overline{\left(\varphi_{,\theta}^{(q)} \right)_{q}} - i \overline{\left(\varphi_{,\theta\theta}^{(q)} \right)_{q}} \right] - b^{(q)} \overline{\left(\psi_{,\theta}^{(q)} \right)_{q}} \right\} + O(h^{2}). \tag{42}$$

Following the same procedure, we obtain the second jump condition across the layer as

$$\sum_{q=1}^{2} (-1)^{q} \left\{ c^{(q)} \overline{\varphi_{q}^{(q)}} + b^{(q)} \left[2i \overline{(\varphi_{,\theta}^{(q)})_{q}} + \overline{(\varphi_{,\theta\theta}^{(q)})_{q}} \right] + d^{(q)} \psi_{q}^{(q)} \right. \\
+ ie^{-2i\theta} \left[\left(a^{(q)} - d^{(q)} \right) \left(\varphi_{,\theta}^{(q)} \right)_{q} - b^{(q)} \overline{(\psi_{,\theta}^{(q)})_{q}} \right] \right\} \\
= -\frac{ih}{2} \sum_{q=1}^{2} \frac{1}{R_{q}} \left\{ c^{(q)} \overline{(\varphi_{,\theta}^{(q)})_{q}} + b^{(q)} \left[2i \overline{(\varphi_{,\theta\theta}^{(q)})_{q}} + \overline{(\varphi_{,\theta\theta\theta}^{(q)})_{q}} \right] + d^{(q)} \left(\psi_{,\theta}^{(q)} \right)_{q} \right. \\
+ e^{-2i\theta} \left[\left(a^{(q)} - d^{(q)} \right) \left[2 \left(\varphi_{,\theta}^{(q)} \right)_{q} + i \left(\varphi_{,\theta\theta}^{(q)} \right)_{q} \right] - b^{(q)} \left[2 \overline{(\psi_{,\theta}^{(q)})_{q}} + i \overline{(\psi_{,\theta\theta}^{(q)})_{q}} \right] \right] \right\} + O(h^{2}). \tag{43}$$

Second step: Jump conditions across the interface

In the second step, we consider two-phase configuration of Fig. 2. To formulate jump conditions across the interface, we assume that conditions (42) and (43) obtained in the first step are valid for the corresponding fields in the two-phase configuration.

We start from expanding the fields involved in (42) in terms of the following Taylor series about $z = z_0$:

$$\varphi^{(q)}(z_q) = \varphi_0^{(q)} + \sum_{k=1}^{\infty} \frac{(R_q - R_0)^k}{k!} \left(\frac{\partial^k \varphi^{(q)}}{\partial r^k}\right)_0,$$

$$\psi^{(q)}(z_q) = \psi_0^{(q)} + \sum_{k=1}^{\infty} \frac{(R_q - R_0)^k}{k!} \left(\frac{\partial^k \psi^{(q)}}{\partial r^k}\right)_0,$$
(44)

and truncate those series up to the first order as

$$\varphi^{(q)}(z_q) = \varphi_0^{(q)} - (-1)^q \frac{ih}{2R_0} \left(\varphi_{,\theta}^{(q)} \right)_0 + O(h^2),$$

$$\psi^{(q)}(z_q) = \psi_0^{(q)} - (-1)^q \frac{ih}{2R_0} \left(\psi_{,\theta}^{(q)} \right)_0 + O(h^2),$$
(45)

where we again used (39) and Cauchy-Riemann conditions (4). Other terms involved in jump condition (42) could be obtained by taking corresponding derivative and applying conjugation to Eqs. (45). Additionally, we expand $1/R_q$ as

$$\frac{1}{R_q} = \left[R_0 \left(1 + (-1)^q \frac{h}{2R_0} \right) \right]^{-1} = \frac{1}{R_0} \left[1 + \sum_{k=1}^{\infty} (-1)^{k(q+1)} \left(\frac{h}{2R_0} \right)^k \right]$$
(46)

and truncate it up to the first two leading terms as

$$\frac{1}{R_q} = \frac{1}{R_0} \left[1 - (-1)^q \frac{h}{2R_0} \right] + O(h^2). \tag{47}$$

Applying expansions (45) and (47) to jump condition (42), neglecting all terms that include h^n with n > 1 (the condition is defined by the order of the interface model), and using straightforward algebra, we get the first jump condition across the interface as

$$\sum_{q=1}^{2} (-1)^{q} \left\{ a^{(q)} \varphi_{0}^{(q)} - b^{(q)} \left[i e^{2i\theta} \overline{\left(\varphi_{,\theta}^{(q)} \right)_{0}} + \overline{\psi_{0}^{(q)}} \right] \right\}
= -\frac{ih}{R_{0}} \sum_{q=1}^{2} b^{(q)} \left\{ e^{2i\theta} \left[\overline{\left(\varphi_{,\theta}^{(q)} \right)_{0}} - i \overline{\left(\varphi_{,\theta\theta}^{(q)} \right)_{0}} \right] - \overline{\left(\psi_{,\theta}^{(q)} \right)_{0}} \right\} + O(h^{2}).$$
(48)

Following similar logic of using expansions (45) and (47) in jump condition (43) and neglecting all terms that include h^n with n > 1, we obtain the second jump condition across the interface as

$$\sum_{q=1}^{2} (-1)^{q} \left\{ c^{(q)} \overline{\varphi_{0}^{(q)}} + b^{(q)} \left[2i \overline{(\varphi_{,\theta}^{(q)})}_{0} + \overline{(\varphi_{,\theta\theta}^{(q)})}_{0} \right] + d^{(q)} \psi_{0}^{(q)} \right. \\
+ i e^{-2i\theta} \left[\left(a^{(q)} - d^{(q)} \right) \left(\varphi_{,\theta}^{(q)} \right)_{0} - b^{(q)} \overline{(\psi_{,\theta}^{(q)})}_{0} \right] \right\} \\
= -\frac{ih}{R_{0}} \sum_{q=1}^{2} \left\{ c^{(q)} \overline{(\varphi_{,\theta}^{(q)})}_{0} + b^{(q)} \left[2i \overline{(\varphi_{,\theta\theta}^{(q)})}_{0} + \overline{(\varphi_{,\theta\theta}^{(q)})}_{0} \right] \right. \\
+ e^{-2i\theta} \left[\left(a^{(q)} - d^{(q)} \right) \left(\varphi_{,\theta}^{(q)} \right)_{0} - b^{(q)} \overline{(\psi_{,\theta}^{(q)})}_{0} + i \overline{(\psi_{,\theta\theta}^{(q)})}_{0} \right] \right] \right\} + O(h^{2}). \tag{49}$$

Eqs. (48) and (49) represent the first order imperfect interface jump conditions for the potentials. Those conditions can be reformulated in terms of jumps in complex displacement and traction across the interface.

Jumps in complex displacement and traction across the interface

Using the derivation presented in detail in Appendix B, we arrive at the following first order jump conditions for the complex displacement and traction:

$$\sigma_{0}^{(2)} - \sigma_{0}^{(1)} = -\frac{2ih}{R_{0}} \sum_{q=1}^{2} \left\{ A_{1}^{(q)} \left[i \operatorname{Re} \left(\sigma_{0}^{(q)} \right) + \operatorname{Re} \left[\left(\sigma_{,\theta}^{(q)} \right)_{0} \right] \right] + \frac{2}{R_{0}} A_{2}^{(q)} \left[-e^{i\theta} \overline{\left(u_{,\theta}^{(q)} \right)_{0}} + \operatorname{Im} \left[e^{-i\theta} \left(u_{,\theta\theta}^{(q)} \right)_{0} \right] \right] \right\} + O(h^{2}),$$

$$u_{0}^{(2)} - u_{0}^{(1)} = -\frac{h}{2R_{0}} e^{i\theta} \sum_{q=1}^{2} \left\{ R_{0} \left[A_{3}^{(q)} \overline{\sigma_{0}^{(q)}} - A_{4}^{(q)} \sigma_{0}^{(q)} \right] + 4A_{1}^{(q)} \operatorname{Im} \left[e^{-i\theta} \left(u_{,\theta}^{(q)} \right)_{0} \right] \right\} + O(h^{2}),$$

$$20$$

$$(50)$$

where $Re[(\cdot)]$ and $Im[(\cdot)]$ refer to the real and imaginary parts of corresponding field and

$$A_{1}^{(q)} = \frac{1}{1 + \kappa^{(0)}} - \frac{1}{1 + \kappa^{(q)}},$$

$$A_{2}^{(q)} = \frac{\mu^{(0)}}{1 + \kappa^{(0)}} - \frac{\mu^{(q)}}{1 + \kappa^{(q)}},$$

$$A_{3}^{(q)} = \frac{1}{\mu^{(0)} (1 + \kappa^{(0)})} - \frac{1}{\mu^{(q)} (1 + \kappa^{(q)})},$$

$$A_{4}^{(q)} = \frac{\kappa^{(0)}}{\mu^{(0)} (1 + \kappa^{(0)})} - \frac{\kappa^{(q)}}{\mu^{(q)} (1 + \kappa^{(q)})}.$$
(51)

If desired, Eqs. (50) can be rewritten in terms of local displacement components by using relation (23).

5.2. List of jump conditions for the second and third order interface models

Using the complex variable implementation of the Bövik-Benveniste methodology similar to that of Section 5.1, but truncating the series at corresponding orders, the jump conditions across the interface for the higher order models can be obtained. Here we list the jump conditions for the third order imperfect interface model, the corresponding conditions for the second order model can be obtained by omitting all terms that are multiplied by h^3 .

The jumps in complex traction and displacement for the third order interface model have

the following forms:

$$\sigma_{0}^{(2)} - \sigma_{0}^{(1)} = -\frac{2ih}{R_{0}} \sum_{q=1}^{2} \left\{ A_{1}^{(q)} \left[i \operatorname{Re} \left(\sigma_{0}^{(q)} \right) + \operatorname{Re} \left[\left(\sigma_{,\theta}^{(q)} \right)_{0} \right] \right] \right. \\
+ \frac{2}{R_{0}} A_{2}^{(q)} \left[-e^{i\theta} \overline{\left(u_{,\theta}^{(q)} \right)_{0}} + \operatorname{Im} \left[e^{-i\theta} \left(u_{,\theta\theta}^{(q)} \right)_{0} \right] \right] \right\} \\
- \frac{h^{2}}{4R_{0}^{2}} \sum_{q=1}^{2} (-1)^{q} \left\{ -B_{4}^{(q)} \operatorname{Re} \left[\sigma_{0}^{(q)} \right] + iB_{2}^{(q)} \overline{\left(\sigma_{,\theta}^{(q)} \right)_{0}} - 4B_{1}^{(q)} \overline{\left(\sigma_{,\theta\theta}^{(q)} \right)_{0}} \right. \\
+ iB_{3}^{(q)} \left(\sigma_{,\theta}^{(q)} \right)_{0} + 2B_{5}^{(q)} \left(\sigma_{,\theta\theta}^{(q)} \right)_{0} + \frac{2e^{i\theta}}{R_{0}} B_{6}^{(q)} \left[2i \overline{\left(u_{,\theta}^{(q)} \right)_{0}} + \overline{\left(u_{,\theta\theta}^{(q)} \right)_{0}} \right] \\
- \frac{2e^{-i\theta}}{R_{0}} \left[B_{7}^{(q)} \left(u_{,\theta\theta}^{(q)} \right)_{0} + 2iB_{8}^{(q)} \left(u_{,\theta\theta\theta}^{(q)} \right)_{0} \right] + 3C_{2}^{(q)} \left[i \overline{\left(\sigma_{,\theta\theta}^{(q)} \right)_{0}} + \overline{\left(\sigma_{,\theta\theta\theta}^{(q)} \right)_{0}} \right] \\
- \frac{h^{3}}{12R_{0}^{3}} \sum_{q=1}^{2} \left\{ 3C_{1}^{(q)} \left[2\operatorname{Re} \left[\sigma_{0}^{(q)} \right] + i \overline{\left(\sigma_{,\theta\theta\theta}^{(q)} \right)_{0}} \right] + 3C_{2}^{(q)} \left[i \overline{\left(\sigma_{,\theta\theta}^{(q)} \right)_{0}} + \overline{\left(\sigma_{,\theta\theta\theta}^{(q)} \right)_{0}} \right] \\
- iC_{3}^{(q)} \left(\sigma_{,\theta}^{(q)} \right)_{0} + 3C_{4}^{(q)} \left(\sigma_{,\theta\theta}^{(q)} \right)_{0} - iC_{5}^{(q)} \left(\sigma_{,\theta\theta\theta}^{(q)} \right)_{0} - \overline{\left(u_{,\theta\theta\theta\theta}^{(q)} \right)_{0}} \right] \\
- \frac{3e^{i\theta}}{R_{0}} C_{6}^{(q)} \left[4i \overline{\left(u_{,\theta\theta}^{(q)} \right)_{0}} + 6\overline{\left(u_{,\theta\theta\theta}^{(q)} \right)_{0}} - 4i \overline{\left(u_{,\theta\theta\theta\theta}^{(q)} \right)_{0}} - \overline{\left(u_{,\theta\theta\theta\theta\theta}^{(q)} \right)_{0}} \right] \\
+ \frac{e^{-i\theta}}{R_{0}} \left[C_{7}^{(q)} \left(u_{,\theta\theta\theta}^{(q)} \right)_{0} + 3iC_{8}^{(q)} \left(u_{,\theta\theta\theta\theta}^{(q)} \right)_{0} - C_{9}^{(q)} \left(u_{,\theta\theta\theta\theta\theta}^{(q)} \right)_{0} \right] \right\} + O(h^{4}),$$

$$u_{0}^{(2)} - u_{0}^{(1)} = -\frac{h}{2R_{0}} e^{i\theta} \sum_{q=1}^{2} \left\{ R_{0} \left[A_{3}^{(q)} \overline{\sigma_{0}^{(q)}} - A_{4}^{(q)} \sigma_{0}^{(q)} \right] + 4A_{1}^{(q)} \operatorname{Im} \left[e^{-i\theta} \left(u_{,\theta}^{(q)} \right)_{0} \right] \right\}$$

$$- \frac{h^{2}}{8R_{0}^{2}} e^{i\theta} \sum_{q=1}^{2} (-1)^{q} \left\{ R_{0} \left[B_{10}^{(q)} \overline{\sigma_{0}^{(q)}} + i B_{9}^{(q)} \overline{\left(\sigma_{,\theta}^{(q)} \right)_{0}} - B_{11}^{(q)} \sigma_{0}^{(q)} + i B_{12}^{(q)} \left(\sigma_{,\theta}^{(q)} \right)_{0} \right] \right\}$$

$$+ 2e^{i\theta} \left[i B_{15}^{(q)} \overline{\left(u_{,\theta}^{(q)} \right)_{0}} - B_{13}^{(q)} \overline{\left(u_{,\theta\theta}^{(q)} \right)_{0}} \right] + 2e^{-i\theta} \left[i B_{14}^{(q)} \left(u_{,\theta}^{(q)} \right)_{0} - B_{16}^{(q)} \left(u_{,\theta\theta}^{(q)} \right)_{0} \right] \right\}$$

$$- \frac{h^{3}}{24R_{0}^{3}} e^{i\theta} \sum_{q=1}^{2} \left\{ R_{0} \left[3C_{10}^{(q)} \left(\overline{\sigma_{0}^{(q)}} - \overline{\left(\sigma_{,\theta\theta}^{(q)} \right)_{0}} \right) + 3iC_{11}^{(q)} \overline{\left(\sigma_{,\theta\theta}^{(q)} \right)_{0}} \right]$$

$$+ 3C_{12}^{(q)} \sigma_{0}^{(q)} + iC_{13}^{(q)} \left(\sigma_{,\theta}^{(q)} \right)_{0} + C_{14}^{(q)} \left(\sigma_{,\theta\theta}^{(q)} \right)_{0} \right]$$

$$+ 3e^{i\theta} \left[C_{15}^{(q)} \left(i \overline{\left(u_{,\theta}^{(q)} \right)_{0}} + \overline{\left(u_{,\theta\theta}^{(q)} \right)_{0}} \right) + iC_{16}^{(q)} \overline{\left(u_{,\theta\theta\theta}^{(q)} \right)_{0}} \right]$$

$$+ 2e^{-i\theta} \left[iC_{17}^{(q)} \left(u_{,\theta}^{(q)} \right)_{0} + 3C_{18}^{(q)} \left(u_{,\theta\theta}^{(q)} \right)_{0} + iC_{19}^{(q)} \left(u_{,\theta\theta\theta}^{(q)} \right)_{0} \right] \right\} + O(h^{4}),$$

where the coefficients related to the terms that are multiplied by h^2 are

$$\begin{split} B_{1}^{(q)} &= \frac{1}{1+\kappa^{(0)}} \left(\frac{\mu^{(0)}}{\mu^{(q)}}-1\right), \qquad B_{2}^{(q)} &= A_{1}^{(q)} - \frac{8}{\kappa^{(q)}+1} B_{1}^{(q)}, \\ B_{3}^{(q)} &= \left(3+\kappa^{(q)}\right) A_{1}^{(q)} - \kappa^{(q)} B_{2}^{(q)}, \qquad B_{4}^{(q)} &= B_{2}^{(q)} + B_{3}^{(q)} - 2A_{1}^{(q)}, \\ B_{5}^{(q)} &= A_{1}^{(q)} + 2B_{1}^{(q)}, \qquad B_{6}^{(q)} &= -A_{2}^{(q)} + \mu^{(q)} \left(A_{1}^{(q)} - B_{2}^{(q)}\right), \\ B_{7}^{(q)} &= 2A_{2}^{(q)} + B_{6}^{(q)}, \qquad B_{8}^{(q)} &= A_{2}^{(q)}, \\ B_{9}^{(q)} &= \frac{4\left(\kappa^{(q)} - \kappa^{(0)}\right)}{\mu^{(0)}\left(\kappa^{(q)} + 1\right)} B_{1}^{(q)}, \qquad B_{10}^{(q)} &= A_{3}^{(q)} - B_{9}^{(q)} + \frac{1}{\mu^{(0)}} \left(B_{3}^{(q)} - 3A_{1}^{(q)}\right), \\ B_{11}^{(q)} &= A_{4}^{(q)} + \frac{4\left(\kappa^{(q)}\kappa^{(0)} + 1\right)}{\mu^{(0)}\left(\kappa^{(q)} + 1\right)} B_{1}^{(q)}, \qquad B_{12}^{(q)} &= A_{4}^{(q)} + B_{11}^{(q)} + \frac{1}{\mu^{(0)}} \left(B_{2}^{(q)} - A_{1}^{(q)}\right), \\ B_{13}^{(q)} &= \frac{4}{1+\kappa^{(q)}} \left(\frac{\mu^{(q)}}{\mu^{(0)}} - 1\right), \qquad B_{14}^{(q)} &= A_{1}^{(q)} - \frac{2}{(\kappa^{(0)} + 1)} B_{13}^{(q)}, \\ B_{15}^{(q)} &= \left(1-\kappa^{(0)}\right) A_{1}^{(q)} + \kappa^{(0)} B_{14}^{(q)}, \qquad B_{16}^{(q)} &= 2A_{1}^{(q)} - B_{13}^{(q)}. \end{split}$$

and the coefficients related to the terms that are multiplied by h^3 are

$$C_{1}^{(q)} = \frac{1}{4} \left(B_{4}^{(q)} - 2A_{1}^{(q)} \right), \qquad C_{2}^{(q)} = C_{1}^{(q)} + A_{1}^{(q)} - B_{2}^{(q)},$$

$$C_{3}^{(q)} = -A_{1}^{(q)} + 12B_{1}^{(q)}, \qquad C_{4}^{(q)} = A_{1}^{(q)} - 2B_{1}^{(q)},$$

$$C_{5}^{(q)} = \frac{1}{2} \left(7A_{1}^{(q)} - 3B_{2}^{(q)} \right), \qquad C_{6}^{(q)} = B_{6}^{(q)} + A_{2}^{(q)},$$

$$C_{7}^{(q)} = 2A_{2}^{(q)} + 9C_{6}^{(q)}, \qquad C_{8}^{(q)} = 2A_{2}^{(q)} + 3C_{6}^{(q)},$$

$$C_{9}^{(q)} = 2A_{2}^{(q)} + C_{8}^{(q)}, \qquad C_{10}^{(q)} = -\frac{1}{2} \left(B_{10}^{(q)} - A_{3}^{(q)} \right),$$

$$C_{11}^{(q)} = -B_{9}^{(q)}, \qquad C_{12}^{(q)} = \frac{1}{2} \left(3B_{11}^{(q)} - A_{4}^{(q)} \right),$$

$$C_{13}^{(q)} = \frac{1}{2} \left(3B_{11}^{(q)} - 6B_{12}^{(q)} + 11A_{4}^{(q)} \right), \qquad C_{14}^{(q)} = \frac{1}{2} \left(3B_{12}^{(q)} - 3B_{11}^{(q)} + A_{4}^{(q)} \right),$$

$$C_{15}^{(q)} = \frac{4\kappa^{(0)}}{\kappa^{(0)} + 1} B_{13}^{(q)}, \qquad C_{16}^{(q)} = \frac{1}{\kappa^{(0)} + 1} B_{13}^{(q)} - \frac{1}{4} C_{15}^{(q)},$$

$$C_{17}^{(q)} = -A_{1}^{(q)} + 9 \left(\frac{1}{4} C_{15}^{(q)} + C_{16}^{(q)} \right), \qquad C_{18}^{(q)} = A_{1}^{(q)} - C_{15}^{(q)} - \frac{7}{2} C_{16}^{(q)},$$

$$C_{19}^{(q)} = 2A_{1}^{(q)} - 3 \left(\frac{1}{4} C_{15}^{(q)} + C_{16}^{(q)} \right).$$

6. Numerical examples

In this Section, we use imperfect interface problem of Fig. 2 with the conditions of Section 5 for the jumps across the interface in order to solve the case study problem of Fig. 1. The solution for the former problem is then compared with the analytical solution of Appendix A for the latter problem.

To solve the imperfect interface problem, we employ the well-known representations for the elastic fields that are available for various cases of uniform far-field loading. The unknown coefficients involved in such representations are then found from the linear systems of algebraic equations that result from the substitution of the representations in the prescribed interface jump conditions such as, e.g., Eqs. (52), (53). Similar procedures were implemented in, e.g., Benveniste (2006b) and Baranova et al. (2020).

6.1. Hydrostatic far-field loading

Consider the case of hydrostatic far-field loading $\sigma_{xx}^{\infty} = \sigma_{yy}^{\infty} = \sigma_h^{\infty}$ and $\sigma_{xy}^{\infty} = 0$. In this case, the problem is one-dimensional. The radial displacements can be represented by the following well-known expressions, reviewed in, e.g., Mogilevskaya et al. (2019):

$$u_r^{(1)}(r) = F_1 r, u_r^{(2)}(r) = F_2 r + F_3 r^{-1}, (56)$$

where F_1 , F_2 , and F_3 are the unknown coefficients. The complex displacements could be simply expressed as $u^{(q)} = u_r^{(q)} e^{i\theta}$ for $q = \{1, 2\}$.

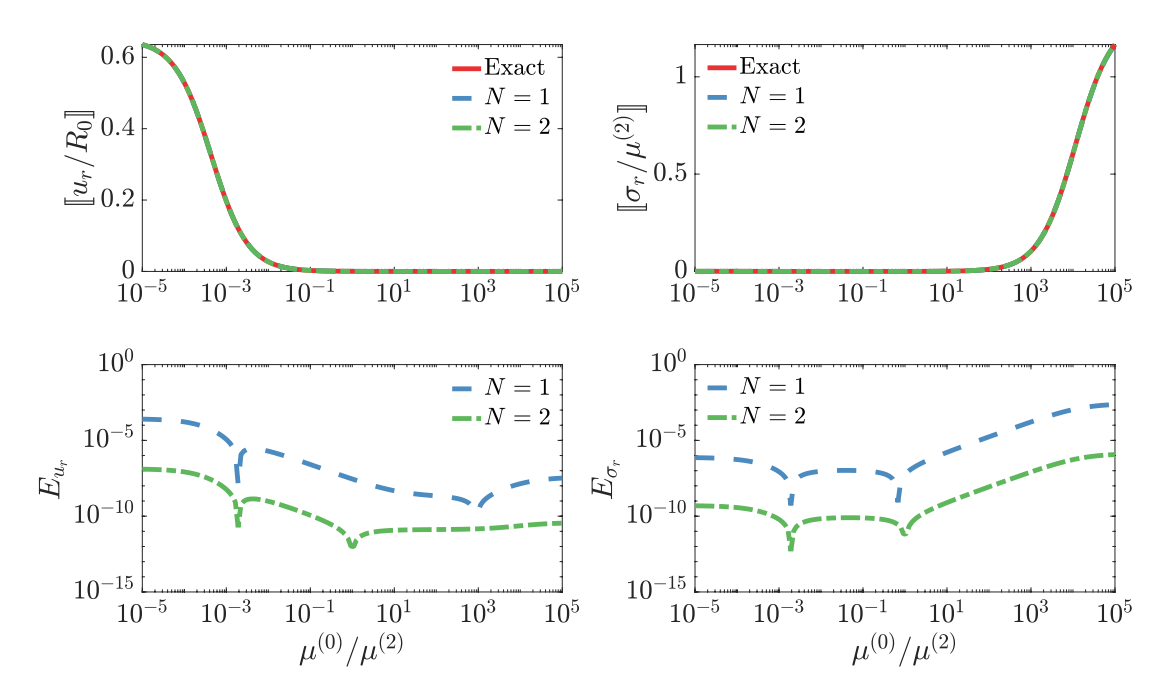


Figure 6: Normalized jumps in radial displacements and tractions and corresponding absolute errors as functions of $\mu^{(0)}/\mu^{(2)}$. Problem-specific parameters are $\sigma_h^{\infty}/\mu^{(2)}=1$, $\mu^{(1)}/\mu^{(2)}=5$, and $\varepsilon=0.001$. (For interpretation of the references to colour in this figure legend, the reader is referred to the Web version of this article. Some of the lines representing fields might be not visible, when they overlapped by the other lines due to the chosen scales of plots.)

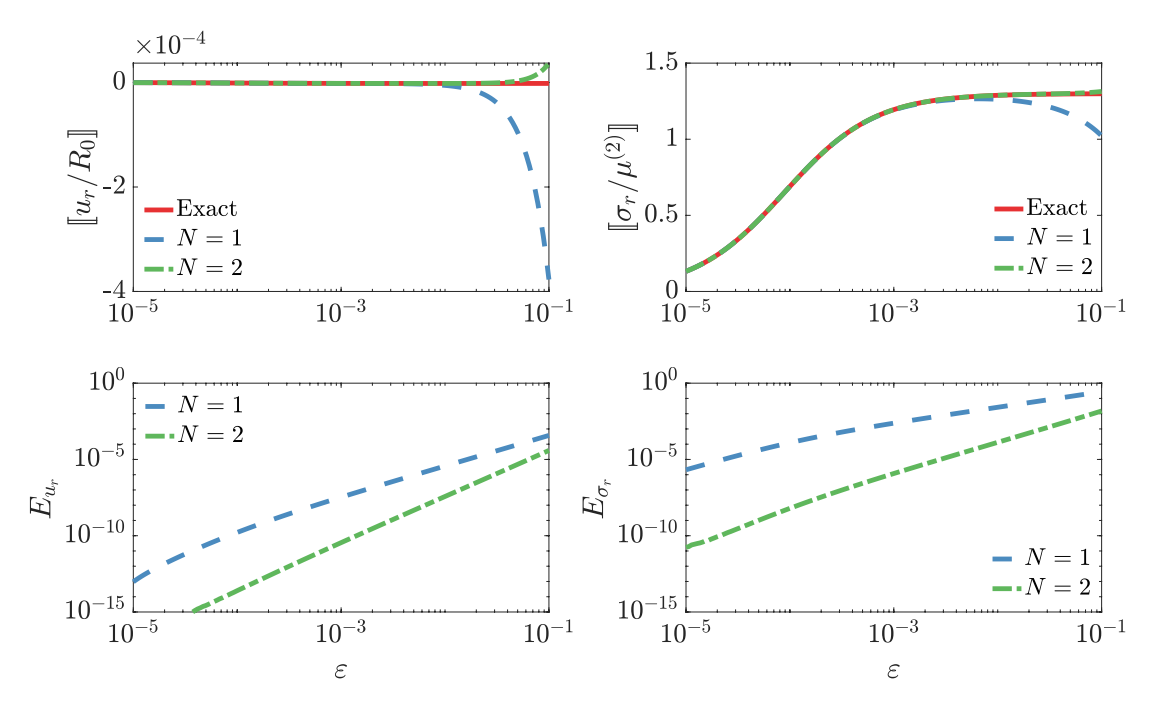


Figure 7: Normalized jumps in radial displacements and tractions and corresponding absolute errors as functions of ε . Problem-specific parameters are $\sigma_h^{\infty}/\mu^{(2)} = 1$, $\mu^{(1)}/\mu^{(2)} = 5$, and $\mu^{(0)}/\mu^{(2)} = 1.3 \cdot 10^5$. (For interpretation of the references to colour in this figure legend, the reader is referred to the Web version of this article.)

The only non-zero traction components can be obtained from Eq. (56) as

$$\sigma_r^{(1)}(r) = \frac{2\mu^{(1)}}{1 - 2\nu^{(1)}} F_1, \qquad \sigma_r^{(2)}(r) = \frac{2\mu^{(2)}}{1 - 2\nu^{(2)}} F_2 - 2\mu^{(2)} F_3 r^{-2}, \tag{57}$$

and the complex tractions are equal to the corresponding radial components $\sigma^{(q)} = \sigma_r^{(q)}$ (for $q = \{1, 2\}$).

The coefficient F_2 can be determined from the far-field condition as

$$F_2 = \frac{1 - 2\nu^{(2)}}{2\mu^{(2)}} \sigma_h^{\infty}. \tag{58}$$

The unknown coefficients F_1 and F_3 can be computed by solving the linear system of algebraic equation obtained from the interface conditions, as described above.

For this problem, we used the jump conditions of the first and second order interface models only and adopted the following set of parameters: $\sigma_h^{\infty}/\mu^{(2)} = 1$, $\mu^{(1)}/\mu^{(2)} = 5$, and $\nu^{(p)} = 0.35$ $(p = \{0, 1, 2\})$.

First, we chose relatively thin layer of $\varepsilon = h/R_0 = 0.001$ and obtained the solutions of the interface models for wide range of $\mu^{(0)}/\mu^{(2)} = [10^{-5}, 10^5]$. Figure 6 plots the normalized jumps in radial displacements and tractions, defined by Eq. (33), and corresponding absolute errors, defined by the relevant equations of Eqs. (34), as functions of the ratio $\mu^{(0)}/\mu^{(2)}$.

It can be seen from Fig. 6 that both models provide accurate results for entire range of $\mu^{(0)}/\mu^{(2)}$ with the second order model showing better accuracy than the first order model. The absolute errors E_{u_r} and E_{σ_r} of the first order model were less than $2.6 \cdot 10^{-4}$ and $2.4 \cdot 10^{-3}$, respectively, while the corresponding absolute errors of the second order model were less than $1.3 \cdot 10^{-7}$ and $1.2 \cdot 10^{-6}$, respectively. We note that the use of absolute errors and logarithmic scale in Fig. 6 makes it look like a significant increase in performance for some values of ratio $\mu^{(0)}/\mu^{(2)}$. However, this phenomenon can be explained by the change in signs of the differences between exact and approximate solutions.

Next, we chose relatively stiff layer of $\mu^{(0)}/\mu^{(2)} = 1.3 \cdot 10^5$ and studied the solutions of the interface models for wide range of $\varepsilon = [10^{-5}, 10^{-1}]$. Figure 7 plots the normalized jumps in radial displacements and tractions, defined by Eq. (33), and corresponding absolute errors, defined by the relevant equations of Eqs. (34), as functions of ε . The exact values of normalized jump in radial displacement for the three-phase case study problem is of order 10^{-6} , while those values for the normalized jump in radial traction is of order 1. The first order model provides accurate results for $[u_r/R_0]$ ($E_{u_r} < 2 \cdot 10^{-7}$) when $\varepsilon < 0.002$ and for $[\sigma_r/R_0]$ ($E_{\sigma_r} < 0.13$) when $\varepsilon < 0.05$. The second order model provides accurate results for wider range of relative thickness: the similar values of $E_{u_r} < 2 \cdot 10^{-7}$ and $E_{\sigma_r} < 0.13$ are obtained for $\varepsilon < 0.017$ and $\varepsilon < 0.094$, respectively. From this example, it is clear that for the case of relatively thick examples, the higher order models are required.

6.2. Simple shear far-field loading

Now we consider the case of simple shear far-field loading $(\sigma_{xx}^{\infty} = -\sigma_{yy}^{\infty} = \sigma_d^{\infty}, \sigma_{xy}^{\infty} = 0)$. In this case, the representations for the elastic fields for the problem of Fig. 2 are given by Eqs. (21), (22), (24), and (25). The unknown coefficients a_1 , d_1 , a_3 , and c_3 can be computed by solving the linear system of algebraic equations obtained from the interface conditions, as described above. We studied this case using the jump conditions of the first, second, and third order models and considered the same examples as those presented in Section 4.1. As before, we adopted the following parameters $\sigma_d^{\infty}/\mu^{(2)} = 1$, $\mu^{(1)}/\mu^{(2)} = 5$, and $\nu^{(p)} = 0.35$ $(p = \{0, 1, 2\})$.

For the first example, we chose relatively thin and soft layer characterised by $\mu^{(0)}/\mu^{(2)} = 1.3 \cdot 10^{-5}$ and $\varepsilon = 0.001$. As mentioned in Section 4.1, for this example, the values of the exact solutions for the normalized jumps $[u_r/R_0]$ and $[u_\theta/R_0]$ are of order 1 and those for $[\sigma_r/\mu^{(2)}]$ and $[\sigma_\theta/\mu^{(2)}]$ are of orders 10^{-7} and 10^{-4} , respectively. The normalized jumps in normal and tangential displacement and traction components and corresponding absolute errors for this example are plotted on Fig. 8. It can be seen that the normalized displacement jumps $[u_r/R_0]$ and $[u_\theta/R_0]$ are accurately approximated by the first order model (N=1) with E_{u_r} and E_{u_θ} being less than $8 \cdot 10^{-4}$. However, the normalized jumps in traction $[\sigma_r/\mu^{(2)}]$ and $[\sigma_\theta/\mu^{(2)}]$ are accurately evaluated only starting from the second order model (N=2) with E_{σ_r} and E_{σ_θ} being less than $7.5 \cdot 10^{-9}$ and $1.6 \cdot 10^{-8}$. The approach of Section 4.1, for this example, provided better accuracy in terms of absolute errors (as it could be expected); however, quantitatively, the imperfect interface models provided similar results.

For the second example, we considered relatively thin and stiff layer with $\mu^{(0)}/\mu^{(2)} = 1.3 \cdot 10^{10}$ and $\varepsilon = 0.001$. For this example (also considered in Section 4.1), the exact

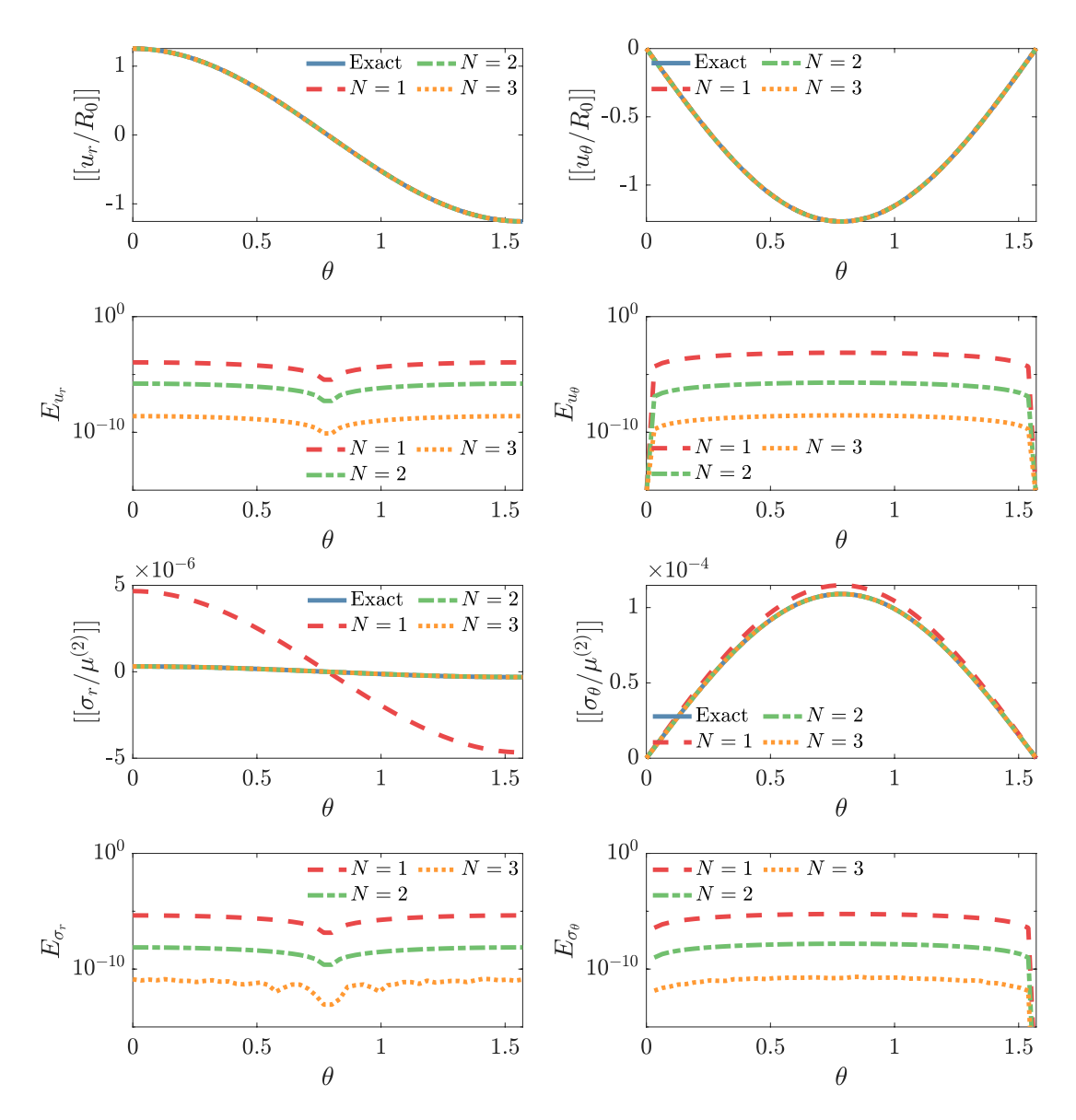


Figure 8: Normalized jumps in displacement and traction components and corresponding absolute errors plotted with respect to θ . Problem-specific parameters are $\sigma_d^{\infty}/\mu^{(2)}=1$, $\mu^{(1)}/\mu^{(2)}=5$, $\mu^{(0)}/\mu^{(2)}=1.3\cdot 10^{-5}$, and $\varepsilon=0.001$. (For interpretation of the references to colour in this figure legend, the reader is referred to the Web version of this article. Some of the lines representing fields might be not visible, when they overlapped by the other lines due to the chosen scales of plots.)

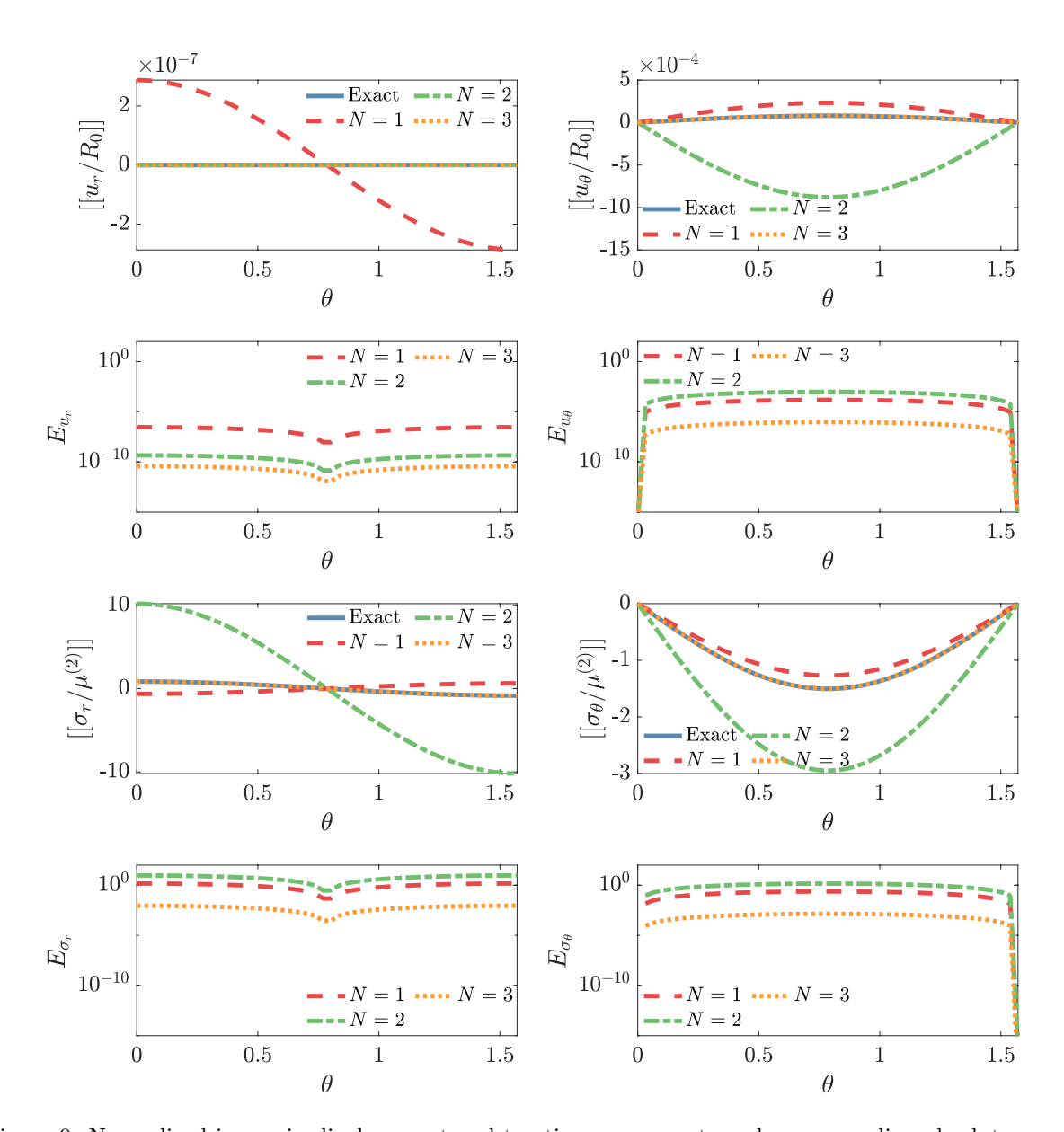


Figure 9: Normalized jumps in displacement and traction components and corresponding absolute errors plotted with respect to θ . Problem-specific parameters are $\sigma_d^\infty/\mu^{(2)}=1$, $\mu^{(1)}/\mu^{(2)}=5$, $\mu^{(0)}/\mu^{(2)}=1.3\cdot 10^{10}$, and $\varepsilon=0.001$. (For interpretation of the references to colour in this figure legend, the reader is referred to the Web version of this article.)

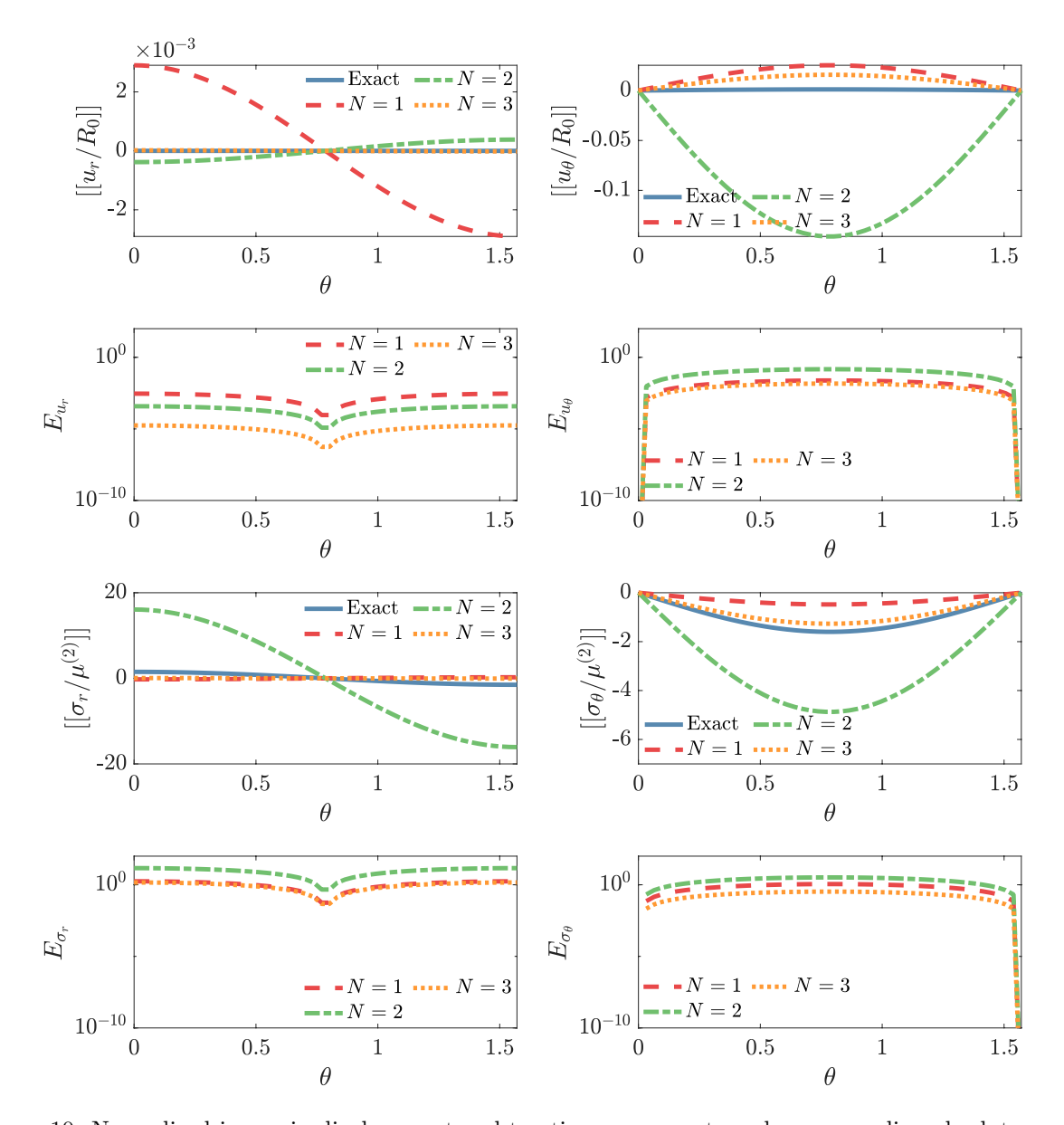


Figure 10: Normalized jumps in displacement and traction components and corresponding absolute errors plotted with respect to θ . Problem-specific parameters are $\sigma_d^{\infty}/\mu^{(2)}=1$, $\mu^{(1)}/\mu^{(2)}=5$, $\mu^{(0)}/\mu^{(2)}=1.3\cdot 10^5$, and $\varepsilon=0.1$. (For interpretation of the references to colour in this figure legend, the reader is referred to the Web version of this article.)

solutions for the normalized jumps $\llbracket u_r/R_0 \rrbracket$ and $\llbracket u_\theta/R_0 \rrbracket$ are given by very small values (they are of order 10^{-12} and 10^{-5} , respectively), while those for $\llbracket \sigma_r/\mu^{(2)} \rrbracket$ and $\llbracket \sigma_\theta/\mu^{(2)} \rrbracket$ are of order 1. The normalized jumps in normal and tangential displacement and traction components and corresponding absolute errors for this example are plotted on Fig. 9. The jump in normalized tangential displacement $\llbracket u_\theta/R_0 \rrbracket$ and the jumps in normalized traction components $\llbracket \sigma_r/\mu^{(2)} \rrbracket$ and $\llbracket \sigma_\theta/\mu^{(2)} \rrbracket$ are accurately approximated starting with the third order model (N=3) with absolute errors E_{u_θ} , E_{σ_r} , and E_{σ_θ} being less than $9.2 \cdot 10^{-7}$, $9 \cdot 10^{-3}$, and $1.4 \cdot 10^{-3}$, respectively. The small values of normalized jump in normal displacement could not be approximated even by the third order model: maximum of absolute error E_{u_r} (among considered range of θ) is around $3.8 \cdot 10^{-11}$. For better accuracy of approximated solutions of the normal displacement, higher order interface models are needed. The approach in Section 4.1, for this example, resulted in better convergence, when the normalized jumps in tractions could be accurately obtained starting from N=1 and the normalized jump in tangential displacement was obtained starting from N=1. For the normalized jump in normal displacement, that approach also required higher order models.

For the third example, we chose relatively thick and stiff layer with $\mu^{(0)}/\mu^{(2)} = 1.3 \cdot 10^5$ and $\varepsilon = 0.1$. Exact solutions for this example (see Section 4.1) are given by very small values of the normalized jumps $\llbracket u_r/R_0 \rrbracket$ and $\llbracket u_\theta/R_0 \rrbracket$ (of order 10^{-7} and 10^{-3} , respectively) and by values of normalized $\llbracket \sigma_r/\mu^{(2)} \rrbracket$ and $\llbracket \sigma_\theta/\mu^{(2)} \rrbracket$ that are of order 1. The normalized jumps in normal and tangential displacement and traction components and the corresponding absolute errors for this example are plotted on Fig. 10. It can be seen that all considered interface models $(N = \{1, 2, 3\})$ do not provide sufficiently accurate results. The third order model provides the best results with the maximum values of absolute errors in corresponding normalized jumps being approximately $E_{u_r} = 1.7 \cdot 10^{-5}$, $E_{u_\theta} = 1.4 \cdot 10^{-2}$, $E_{\sigma_r} = 1.45$, $E_{\sigma_\theta} = 0.33$. It can be concluded that for thick and stiff layers, high order interface models are required.

We note that the results for the third example, obtained with the imperfect interface models, were quite different from those obtained with the approach of Section 4.1. The latter approach had much faster convergence rate (N=1 provided accurate results for $\llbracket \sigma_r/\mu^{(2)} \rrbracket$ and $\llbracket \sigma_\theta/\mu^{(2)} \rrbracket$), N=2 was sufficient to accurately evaluate $\llbracket u_\theta/R_0 \rrbracket$, and higher orders $(N \geq 6)$ were only required for accurate evaluation of $\llbracket u_r/R_0 \rrbracket$. Such difference could be expected for this extreme example as the imperfect interface-based approach does not use any prior information on the solutions for the case study problem, while the approach of Section 4.1 employs the exact solutions at some point.

Finally, we would like to highlight the fact that in the last two examples, the results obtained with the second order imperfect interface model were less accurate than those obtained with the first order model. Similar observation was made in Benveniste and Berdichevsky (2010). The reason for why this is the case remains unclear. However, according to the classification of Benveniste and Miloh (2001), the considered material parameters for the case are consistent with the so-called "inextensible shell type" regime, defined by Eqs. (2.15) and (2.16) of the latter paper. It could be concluded from those equations that i) the condition for jumps in traction components involve higher order derivatives that are only present in the third order jump conditions; ii) parameter D involved in Eqs. (2.16) includes the term

 h^3 that is present only in the models of third order. Thus, it is clear that the inextensible shell type interface regime could only be recovered from the third order model.

6.3. More general uniform far-field loading

As an example, we consider the case study problem under uniaxial far-field loading and present the results for the elastic displacements and stresses inside the composite system.

We choose uniaxial far-field load with the following components:

$$\{\sigma_{xx}^{\infty}, \sigma_{yy}^{\infty}, \sigma_{xy}^{\infty}\}/\mu^{(2)} = \{1, 0, 0\}$$
 (59)

and consider the case of a thin $(\varepsilon = 0.001)$ and stiff $(\mu^{(0)}/\mu^{(2)} = 1.3 \cdot 10^{10})$ layer. The remaining problem parameters were taken to be $\mu^{(1)}/\mu^{(2)} = 5$, $\nu^{(p)} = 0.35$ $(p = \{0, 1, 2\})$. We mention that the same problem parameters were used in Subsection 6.2 for the case of simple shear far-field loading.

Exact solutions for the elastic fields inside the fiber and the matrix in three-phase configuration are obtained using Kolosov-Muskhelishvili farmulae (13) and the potentials provided in Appendix A.3 assuming the loading in the form of (59).

Solution of the problem in two-phase configuration is obtained by superposing the solutions for hydrostatic and simple shear far-field loadings. Elastic fields in the fiber and in the matrix are obtained as sums of the corresponding third order interface models' solutions (N=3) for hydrostatic $(\sigma_h^{\infty}=1/2)$ and simple shear $(\sigma_d^{\infty}=1/2)$ far-field loading described in Sections 6.1 and 6.2.

Figure 11 plots displacement components u_r and u_θ and radial and shear stress components σ_{rr} and $\sigma_{r\theta}$ along three radial directions $\theta = \{0, \pi/4, \pi/2\}$. It can be seen from the figure that the third order model accurately approximates exact solutions. To gain better insight on accuracy of our approach, we also present the results in Table 1, which contains the values for the fields at the points located inside the fiber, the matrix $(r/R_0 = 0.6, r/R_0 = 1.4)$, and at the traces of the layer boundaries $(r/R_0 = 0.9995, r/R_0 = 1.0005)$ along previously chosen radial directions $(\theta = \{0, \pi/4, \pi/2\})$. It can be concluded that the third order model can accurately capture four significant digits of the exact solutions. We add that the results for the fields inside the layer, 0.9995 $< r/R_0 < 1.0005$, are not presented. Similar as for harmonic problems, see Baranova et al. (2020), they could be accurately recovered from the solution of separate problem containing an annual region (that represents the layer) with the prescribed conditions at its boundaries obtained for the two-phase configuration problem at the traces of layer boundary.

Finally, we would like to add the following remark. Even though the series for jump conditions for interface model of order N are truncated up to $O(h^{N+1})$, the errors of computed elastic fields are not necessarily of the same orders. In fact, the remaining terms of series might contain multiplayers such as, e.g., normalized shear modulus of the layer $\mu^{(0)}/\mu^{(2)}$. The orders of such multiplyers could be comparable with ε^{-N} and that could increase the errors of the solutions. This effect could be observed for the problem considered in this subsection, where the errors of the solutions obtained with the third order models were of orders $O(\varepsilon)$. Further investigation are needed to study the influence of elastic parameters of layer material on accuracy of interface models.

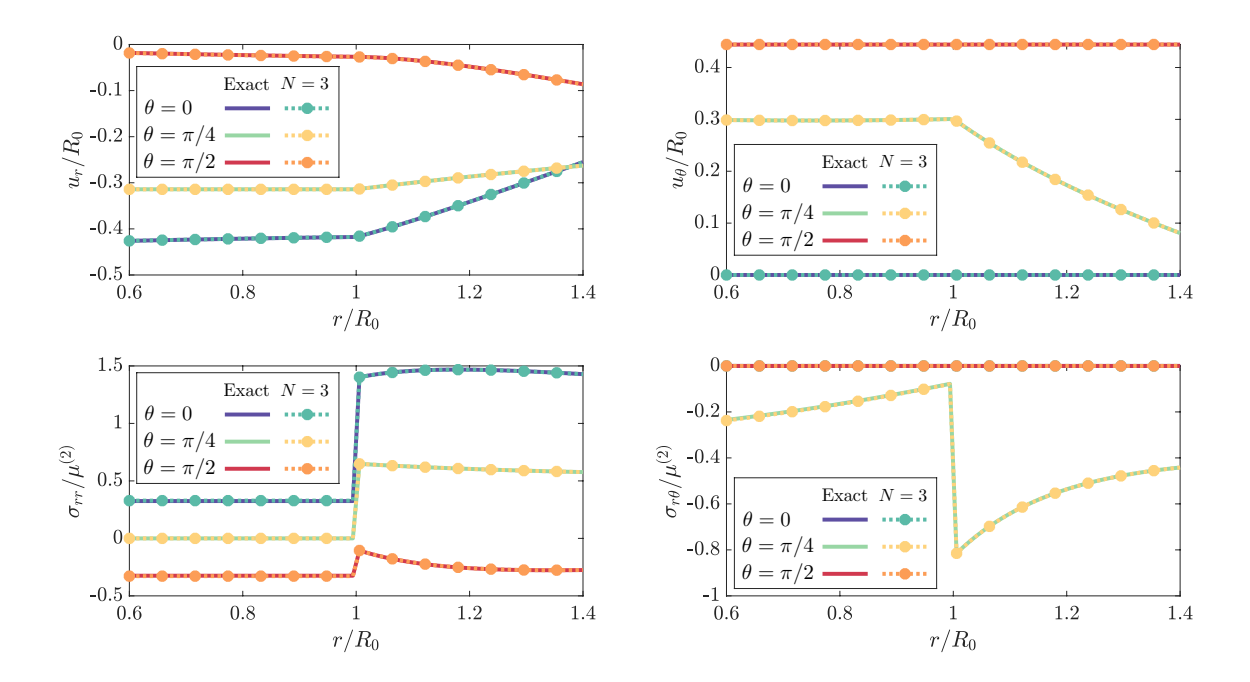


Figure 11: Normalized displacements and stress components with respect to r/R_0 . Problem-specific parameters are $\{\sigma_{xx}^{\infty}, \sigma_{yy}^{\infty}, \sigma_{xy}^{\infty}\}/\mu^{(2)} = \{1,0,0\}, \ \mu^{(1)}/\mu^{(2)} = 5, \ \mu^{(0)}/\mu^{(2)} = 1.3 \cdot 10^{10}, \ \text{and} \ \varepsilon = 0.001$. (For interpretation of the references to colour in this figure legend, the reader is referred to the Web version of this article.)

Coordinate		u_r/R_0		u_{θ}/R_0		$\sigma_{rr}/\mu^{(2)}$		$\sigma_{r\theta}/\mu^{(2)}$	
r/R_0	θ	Exact	N=3	Exact	N=3	Exact	N = 3	Exact	N=3
0.6	0	-0.426	-0.426	0	0	0.3247	0.3284	0	0
0.6	$\pi/4$	-0.3141	-0.3142	0.2988	0.2987	0	0	-0.2348	-0.2375
0.6	$\pi/2$	-0.0182	-0.0184	0.4442	0.4444	-0.3247	-0.3284	0	0
0.9995	0	-0.4176	-0.4174	0	0	0.3247	0.3284	0	0
0.9995	$\pi/4$	-0.3141	-0.3142	0.3008	0.3007	0	0	-0.0752	-0.0761
0.9995	$\pi/2$	-0.0266	-0.0269	0.4442	0.4444	-0.3247	-0.3284	0	0
1.0005	0	-0.4176	-0.4174	0	0	1.3976	1.3968	0	0
1.0005	$\pi/4$	-0.3141	-0.3142	0.3008	0.3008	0.65	0.65	-0.8275	-0.8277
1.0005	$\pi/2$	-0.0266	-0.0269	0.4442	0.4444	-0.0976	-0.0968	0	0
1.4	0	-0.2552	-0.2551	0	0	1.4286	1.4281	0	0
1.4	$\pi/4$	-0.2627	-0.2629	0.0807	0.0808	0.5766	0.5766	-0.4417	-0.4419
1.4	$\pi/2$	-0.0863	-0.0865	0.4442	0.4444	-0.2754	-0.2749	0	0

Table 1: Normalized displacements and stress components.

7. Conclusion

In this work, we performed two-dimensional case study of the Bövik-Benveniste methodology for modeling elastic imperfect interfaces. The study produced three following important contributions.

First, we demonstrated, using the case study, that the assumption of the Bövik-Benveniste methodology (that, at its second step, the medium of the layer of the three-phase configuration can be replaced with the corresponding media of remaining two phases and the fields outside the layer can be expanded to the interface to accurately simulate the layer) is valid for a wide range of problem parameters, and that this can be done with any desirable degree of accuracy by increasing truncation number of Taylor series.

Second, we developed novel complex variables-based implementation of the Bövik-Benveniste methodology for the case study problem. Using this implementation, we derived the interface models up to the third order with explicit expressions for the jump conditions. To our best knowledge, the third order model for this methodology is derived here for the first time.

Third, we performed extensive comparisons of the results obtained with the developed models with the corresponding analytical solutions for the case study problem and a wide range of problem parameters. In addition to plotted results, we provided tabulated data that can be used as benchmarks for further investigators. We demonstrated that the issue related to modeling of very stiff layers, raised in Benveniste and Berdichevsky (2010), can be resolved with the use of the higher order models. Thus, the Bövik-Benveniste methodology, indeed, allows for construction of elastic interface models that behave satisfactorily at all ranges of layer stiffness.

The plans for our future work are as follows. As the results obtained here (e.g. explicit forms of jump conditions, etc.) contain enormous information, we plan to use them for further studies of interface models, including identifications of interface regimes and various connections to the low-dimensional- (e.g. rods, beam, etc.) and the material surfaces

theories. While here we focused on two-dimensional problem, three-dimensional problem involving spherical interface could be analysed in similar manner. Finally, similarly as in Baranova et al. (2020), we plan to generalize the complex variables implementation of the methodology to model the problems involving interfaces of arbitrary smooth curvatures.

Acknowledgement

This work was supported by the National Science Foundation (grant number NSF CMMI-2112894). The first author (S.B.) gratefully acknowledges the Hsiao Shaw-Lundquist Fellowship granted by the University of Minnesota China Center. The second authors (S.M.) gratefully acknowledges the support from the Theodore W. Bennett Chair, University of Minnesota.

Appendix A. Analytical solution for the three-phase configuration problem

For the reader convenience, we review the analytical solution for three-phase configuration below. Such solutions are reported in several publications, see e.g. (Ru, 1999; Sudak and Mioduchowski, 2002; Mogilevskaya and Crouch, 2004; Mogilevskaya et al., 2018) for the reviews. Most of them are not well suited for the analysis of various parameters governing the problem, as they involve numerically obtained coefficients. In this work, we use the solution obtained in Mogilevskaya and Crouch (2004), see also Mogilevskaya et al. (2018), which contains only closed-form expressions.

Appendix A.1. Governing coefficients

The solution of Mogilevskaya and Crouch (2004); Mogilevskaya et al. (2018) can be expressed via the following complex coefficients:

$$B_{-21} = -\frac{\left(\kappa^{(2)} + 1\right) \left(a_{22} + a_{32}\right) \sigma_{2}^{\infty}}{8\mu^{(2)}\Delta},$$

$$B_{01} = -\frac{4\sigma_{1}^{\infty}\Delta}{\sigma_{2}^{\infty}\Delta_{1}} B_{-21};$$

$$B_{21} = -\frac{3a_{11}a_{12}\beta \left(\beta - 1\right)}{\Lambda} \overline{B}_{-21},$$

$$B_{-22} = -\frac{2}{c_{12}} \left[\frac{\left(\kappa^{(2)} + 1\right)\sigma_{2}^{\infty}}{4\mu^{(2)}} + a_{11}\beta B_{-21} \right],$$

$$B_{02} = -\frac{\left(\kappa^{(2)} + 1\right) \left[c_{21} - 2\left(2a_{11} - a_{31}\right)\beta\right]\sigma_{1}^{\infty}}{2\mu^{(2)}\Delta_{1}},$$

$$B_{22} = -\frac{c_{31}}{2a_{12}\beta} B_{21},$$
(A.1)

where $\beta = (R_1/R_2)^2$,

$$\Lambda = a_{12} (a_{11} - a_{31}) \beta^2 - \frac{c_{31}c_{32}}{4\beta},$$

$$\Delta = \frac{c_{12}}{4} \left[c_{11} + \frac{3c_{31}a_{11}a_{12}}{\Lambda} (\beta - 1)^2 \right] - a_{11} (a_{12} - a_{32}) \beta,$$

$$\Delta_1 = c_{21}c_{22} - 8a_{12} (2a_{11} - a_{31}) \beta,$$
(A.2)

and a_{kj} and c_{kj} are

$$a_{11} = \frac{1}{2\mu^{(1)}} - \frac{1}{2\mu^{(0)}}, \quad a_{21} = \frac{1+\kappa^{(1)}}{2\mu^{(1)}} + \frac{1+\kappa^{(0)}}{2\mu^{(0)}}, \quad a_{31} = \frac{1+\kappa^{(1)}}{2\mu^{(1)}} - \frac{1+\kappa^{(0)}}{2\mu^{(0)}},$$

$$a_{12} = \frac{1}{2\mu^{(0)}} - \frac{1}{2\mu^{(2)}}, \quad a_{22} = \frac{1+\kappa^{(0)}}{2\mu^{(0)}} + \frac{1+\kappa^{(2)}}{2\mu^{(2)}}, \quad a_{32} = \frac{1+\kappa^{(0)}}{2\mu^{(0)}} - \frac{1+\kappa^{(2)}}{2\mu^{(2)}},$$
(A.3)

$$c_{1j} = 2a_{1j} + a_{2j} - a_{3j}, \quad c_{2j} = 4a_{1j} - a_{2j} - a_{3j}, \quad c_{3j} = 2a_{1j} - a_{2j} - a_{3j}.$$
 (A.4)

The Kolosov-Muskhelishvili potentials for the case problem expressed in terms of those coefficients are presented in Appendix A.3. Thus, all elastic fields inside the fiber, the coating layer, and the matrix could be obtained in terms of the coefficients using Eqs. (A.12)-(A.14) and Eqs. (13).

The complex displacements and tractions at the layers boundaries have the following, particularly simple forms:

$$\sigma^{(q)}(z)\big|_{|z|=R_q} = \sigma^{(0)}(z)\big|_{|z|=R_q} = B_{-2q}e^{-2i\theta} + B_{0q} + B_{2q}e^{2i\theta},$$

$$u^{(q)}(z)\big|_{|z|=R_q} = u^{(0)}(z)\big|_{|z|=R_q} = A_{-1q}e^{-i\theta} + A_{1q}e^{i\theta} + A_{3q}e^{3i\theta},$$

$$q = 1, 2, \qquad (A.5)$$

where coefficients A_{-1q} , A_{1q} , and A_{3q} could be expressed via coefficients B_{-2q} , B_{0q} , and B_{2q}

$$\begin{split} A_{-11} &= -\frac{R_1}{1+\kappa^{(1)}} \left[\frac{1+\kappa^{(2)}}{4\mu^{(2)}} \sigma_2^{\infty} - a_{12} \overline{B}_{22} \left(1-\beta \right) \right. \\ &+ \left(a_{11} - a_{31} \right) B_{-21} + \left(a_{12} - a_{32} \right) B_{-22} \right], \\ A_{11} &= \frac{R_1 \left(\kappa^{(1)} - 1 \right)}{1+\kappa^{(1)}} \left(\frac{1+\kappa^{(2)}}{8\mu^{(2)}} \sigma_1^{\infty} + a_{11} B_{01} + a_{12} B_{02} \right), \\ A_{31} &= \frac{R_1 \kappa^{(1)}}{3 \left(1+\kappa^{(1)} \right)} \left(a_{11} B_{21} + a_{12} B_{22} \beta \right), \\ A_{-12} &= \frac{R_2}{1+\kappa^{(2)}} \left[-\frac{1+\kappa^{(2)}}{4\mu^{(2)}} \sigma_2^{\infty} + \kappa^{(2)} \left(a_{11} B_{-21} \beta + a_{12} B_{-22} \right) \right], \\ A_{12} &= \frac{R_2}{1+\kappa^{(2)}} \left[\frac{\left(\kappa^{(2)} \right)^2 - 1}{8\mu^{(2)}} \sigma_1^{\infty} + \left(a_{31} - 2a_{11} \right) B_{01} \beta + \left(a_{32} - 2a_{12} \right) B_{02} \right], \\ A_{32} &= \frac{R_2}{3 \left(1+\kappa^{(2)} \right)} \left[3a_{11} \overline{B}_{-21} \beta \left(1-\beta \right) - \left(a_{11} - a_{31} \right) B_{21} \beta^2 - \left(a_{12} - a_{32} \right) B_{22} \right]. \end{split}$$

In the cases (studied below in more detail) of hydrostatic ($\sigma_{xx}^{\infty} = \sigma_{yy}^{\infty} = \sigma_h^{\infty}$, $\sigma_{xy}^{\infty} = 0$) and simple shear ($\sigma_{xx}^{\infty} = -\sigma_{yy}^{\infty} = \sigma_d^{\infty}$, $\sigma_{xy}^{\infty} = 0$), far-field loadings, the coefficients are

• Hydrostatic load

$$B_{01} = \frac{\left(\kappa^{(2)} + 1\right) \left(a_{22} + a_{32}\right) \sigma_h^{\infty}}{\mu^{(2)} \Delta_1},$$

$$B_{02} = -\frac{\left(\kappa^{(2)} + 1\right) \left[c_{21} - 2\left(2a_{11} - a_{31}\right)\beta\right] \sigma_h^{\infty}}{\mu^{(2)} \Delta_1},$$

$$B_{-21} = B_{21} = B_{-22} = B_{22} = 0;$$
(A.7)

• Simple shear load

$$B_{-21} = \frac{\left(\kappa^{(2)} + 1\right) \left(a_{22} + a_{32}\right) \sigma_d^{\infty}}{4\mu^{(2)} \Delta},$$

$$B_{21} = -\frac{3a_{11}a_{12}\beta \left(\beta - 1\right)}{\Lambda} \overline{B}_{-21},$$

$$B_{-22} = \frac{2}{c_{12}} \left[\frac{\left(\kappa^{(2)} + 1\right) \sigma_d^{\infty}}{2\mu^{(2)}} - a_{11}\beta B_{-21} \right],$$

$$B_{22} = -\frac{c_{31}}{2a_{12}\beta} B_{21},$$

$$B_{01} = B_{02} = 0.$$
(A.8)

Appendix A.2. Discussion of the analytical solution

Analysis of the expressions of Appendix A.1 suggests that the solution for the case problem is governed by several combinations of the elastic constants of the three media and by the geometrical parameter β . This parameter is the only one that includes the layer thickness h; it could be expressed via h in different ways, e.g. in the finite closed form as

$$\beta = \left(1 - \frac{h}{R_2}\right)^2 \tag{A.9}$$

or in the form of infinite series as

$$\beta = \left[\sum_{k=0}^{\infty} (-1)^k \left(\frac{h}{R_1}\right)^k\right]^2 \tag{A.10}$$

Additionally, by introducing $R_0 = (R_1 + R_2)/2$ as a radius of the mid-line of layer's cross-section, the parameter β could be expressed as

$$\beta = \left(1 - \frac{h}{2R_0}\right)^2 \left[\sum_{k=0}^{\infty} (-1)^k \left(\frac{h}{2R_0}\right)^k\right]^2.$$
 (A.11)

Appendix A.3. Analytical representations for Kolosov-Muskhelishvili potentials

For the case problem, the expressions for the Kolosov-Muskhelishvili potentials in terms of coefficients B_{-2q} , B_{0q} , and B_{2q} are

(i) inside the fiber $(|z| \le R_1)$

$$\varphi^{(1)}(z) = \varphi^{\infty}(z) + \frac{2\mu^{(1)}}{\kappa^{(1)} + 1} \sum_{q=1}^{2} a_{1q} z \left(B_{0q} + B_{2q} \frac{z^2}{3R_q^2} \right),$$

$$\psi^{(1)}(z) = \psi^{\infty} - \frac{2\mu^{(1)}}{\kappa^{(1)} + 1} \sum_{q=1}^{2} z \left[a_{1q} B_{2q} + (a_{3q} - a_{1q}) \overline{B}_{-2q} \right];$$
(A.12)

(ii) inside the coating layer $(R_1 \le |z| < R_2)$

$$\varphi^{(0)}(z) = \varphi^{\infty}(z) + \frac{2\mu^{(0)}}{\kappa^{(0)} + 1} \left[a_{11}B_{-21}\frac{R_1^2}{z} + a_{12}z \left(B_{02} + B_{22}\frac{z^2}{3R_2^2} \right) \right],$$

$$\psi^{(0)}(z) = \psi^{\infty} + \frac{2\mu^{(0)}}{\kappa^{(0)} + 1} \left\{ (2a_{11} - a_{31}) B_{01}\frac{R_1^2}{z} + \frac{R_1^4}{z^3} \left[a_{11}B_{-21} + (a_{11} - a_{31}) \frac{\overline{B}_{21}}{3} \right] + z \left[-a_{12}B_{22} + (a_{12} - a_{32}) \overline{B}_{-22} \right] \right\};$$
(A.13)

(iii) inside the matrix $(|z| \ge R_2)$

$$\varphi^{(2)}(z) = \varphi^{\infty}(z) + \frac{2\mu^{(2)}}{\kappa^{(2)} + 1} \sum_{q=1}^{2} a_{1q} B_{-2q} \frac{R_q^2}{z},$$

$$\psi^{(2)}(z) = \psi^{\infty} + \frac{2\mu^{(2)}}{\kappa^{(2)} + 1} \sum_{q=1}^{2} \left\{ (2a_{1q} - a_{3q}) B_{0q} \frac{R_q^2}{z} + \frac{R_q^4}{z^3} \left[a_{1q} B_{-2q} + (a_{1q} - a_{3q}) \frac{\overline{B}_{2q}}{3} \right] \right\}.$$
(A.14)

Appendix B. Details of the derivations for the first order interface jumps in complex displacement, traction, and resultant force

First, by use of Kolosov-Muskhelishvili formulae (15), the jumps of Eqs. (48) and (49), and Eqs. (36), we obtain the following expressions:

$$\sum_{q=1}^{2} (-1)^{q} \left(f_{0}^{(q)} + 2\mu^{(0)} u_{0}^{(q)} \right) = \frac{ih}{R_{0}} \sum_{q=1}^{2} \frac{b^{(q)}}{(1+\kappa^{(q)})} \left\{ \kappa^{(q)} \left(f_{,\theta}^{(q)} \right)_{0} - 2\mu^{(q)} \left(u_{,\theta}^{(q)} \right)_{0} + e^{2i\theta} \left[\overline{\left(f_{,\theta}^{(q)} \right)_{0}} + 2\mu^{(q)} \overline{\left(u_{,\theta}^{(q)} \right)_{0}} \right] \right\} + O(h^{2}),$$
(B.1)

$$\sum_{q=1}^{2} (-1)^{q} \left\{ \kappa^{(0)} \overline{f_{0}^{(q)}} - 2\mu^{(0)} \overline{u_{0}^{(q)}} + ie^{-2i\theta} \left[\left(f_{,\theta}^{(q)} \right)_{0} + 2\mu^{(0)} \left(u_{,\theta}^{(q)} \right)_{0} \right] \right\}$$

$$= \frac{ih}{R_{0}} \sum_{q=1}^{2} \frac{1}{(1 + \kappa^{(q)})} \left\{ e^{-2i\theta} \left[\left(d^{(q)} - 1 - \kappa^{(q)} \right) \left(f_{,\theta}^{(q)} \right)_{0} + 2\mu^{(q)} c^{(q)} \left(u_{,\theta}^{(q)} \right)_{0} \right. \right.$$

$$+ ib^{(q)} \left(\kappa^{(q)} \left(f_{,\theta\theta}^{(q)} \right)_{0} - 2\mu^{(q)} \left(u_{,\theta\theta}^{(q)} \right)_{0} \right) \left[- \left(2b^{(q)} + c^{(q)} \right) \left[\overline{\left(f_{,\theta}^{(q)} \right)_{0}} + 2\mu^{(q)} \overline{\left(u_{,\theta}^{(q)} \right)_{0}} \right] \right.$$

$$+ ib^{(q)} \left[\overline{\left(f_{,\theta\theta}^{(q)} \right)_{0}} + 2\mu^{(q)} \overline{\left(u_{,\theta\theta}^{(q)} \right)_{0}} \right] \right\} + O(h^{2}). \tag{B.2}$$

Next, we take the derivative of Eq. (B.1) with respect to θ , multiply the result by $ie^{-2i\theta}$, and subtract the resultant equation from Eq. (B.2). Conjugation of the result of those

operations leads us to

$$\sum_{q=1}^{2} (-1)^{q} \left\{ \kappa^{(0)} f_{0}^{(q)} - 2\mu^{(0)} u_{0}^{(q)} \right\}
= -\frac{ih}{R_{0}} \sum_{q=1}^{2} \frac{1}{(1+\kappa^{(q)})} \left\{ -c^{(q)} \left[\left(f_{,\theta}^{(q)} \right)_{0} + 2\mu^{(0)} \left(u_{,\theta}^{(q)} \right)_{0} \right] \right.
+ e^{2i\theta} \left[\left(d^{(q)} - 1 - \kappa^{(q)} \right) \overline{\left(f_{,\theta}^{(q)} \right)_{0}} + 2\mu^{(q)} c^{(q)} \overline{\left(u_{,\theta}^{(q)} \right)_{0}} \right] \right\} + O(h^{2}).$$
(B.3)

Final expressions for the jumps in complex displacement and resultant force can be obtained using Eqs. (B.1), (B.3), and straightforward algebra as

$$f_0^{(2)} - f_0^{(1)} = \frac{2h}{R_0} e^{i\theta} \sum_{q=1}^{2} \left\{ A_1^{(q)} \operatorname{Im} \left[e^{-i\theta} \left(f_{,\theta}^{(q)} \right)_0 \right] + 2A_2^{(q)} \operatorname{Im} \left[e^{-i\theta} \left(u_{,\theta}^{(q)} \right)_0 \right] \right\} + O(h^2),$$

$$u_0^{(2)} - u_0^{(1)} = \frac{ih}{2R_0} \sum_{q=1}^{2} \left\{ -A_3^{(q)} e^{2i\theta} \overline{\left(f_{,\theta}^{(q)} \right)_0} - A_4^{(q)} \left(f_{,\theta}^{(q)} \right)_0 + 4iA_1^{(q)} e^{i\theta} \operatorname{Im} \left[e^{-i\theta} \left(u_{,\theta}^{(q)} \right)_0 \right] \right\} + O(h^2).$$

$$(B.4)$$

By taking the complex derivative of the first expression in (B.4) and using Eq. (9), it is possible to reformulate the jump conditions in terms of complex displacement and traction. These conditions are given by Eqs. (50).

References

Ahlfors, L.V., 1979. Complex analysis: an introduction to the theory of analytic functions of one complex variable. International series in pure and applied mathematics. 3d ed. ed., McGraw-Hill, New York.

Baranova, S., Mogilevskaya, S., Nguyen, T., Schillinger, D., 2020. Higher-order imperfect interface modeling via complex variables based asymptotic analysis. International Journal of Engineering Science 157, 103399.

Benveniste, Y., 2006a. A general interface model for a three-dimensional curved thin anisotropic interphase between two anisotropic media. Journal of the Mechanics and Physics of Solids 54, 708–734.

Benveniste, Y., 2006b. An $O(h^N)$ interface model of a three-dimensional curved interphase in conduction phenomena. Proceedings of the Royal Society A: Mathematical, Physical and Engineering Sciences 462, 1593–1617.

Benveniste, Y., Berdichevsky, O., 2010. On two models of arbitrarily curved three-dimensional thin interphases in elasticity. International Journal of Solids and Structures 47, 1899–1915.

Benveniste, Y., Miloh, T., 2001. Imperfect soft and stiff interfaces in two-dimensional elasticity. Mechanics of materials 33, 309–323.

Bövik, P., 1994. On the modelling of thin interface layers in elastic and acoustic scattering problems. The Quarterly Journal of Mechanics and Applied Mathematics 47, 17–42.

Bövik, P., Olsson, P., 1992. Effective boundary conditions for the scattering of two-dimensional SH waves from a curved thin elastic layer. Proceedings of the Royal Society of London. Series A: Mathematical and Physical Sciences 439, 257–269.

- Christensen, R., Lo, K., 1979. Solutions for effective shear properties in three phase sphere and cylinder models. Journal of the Mechanics and Physics of Solids 27, 315–330.
- Christensen, R.M., 2012. Mechanics of composite materials. Courier Corporation.
- Dumont, S., Lebon, F., Raffa, M.L., Rizzoni, R., Welemane, H., 2016. Multiscale modeling of imperfect interfaces and applications, in: Computational methods for solids and fluids. Springer, pp. 81–122.
- Firooz, S., Steinmann, P., Javili, A., 2021. Homogenization of composites with extended general interfaces: Comprehensive review and unified modeling. Applied Mechanics Reviews.
- Gu, S., Monteiro, E., He, Q.C., 2011. Coordinate-free derivation and weak formulation of a general imperfect interface model for thermal conduction in composites. Composites science and technology 71, 1209–1216.
- Hashin, Z., 2001. Thin interphase/imperfect interface in conduction. Journal of Applied Physics 89, 2261–2267.
- Hashin, Z., 2002. Thin interphase/imperfect interface in elasticity with application to coated fiber composites. Journal of the Mechanics and Physics of Solids 50, 2509–2537.
- Javili, A., McBride, A., Steinmann, P., 2013. Thermomechanics of solids with lower-dimensional energetics: On the importance of surface, interface, and curve structures at the nanoscale. a unifying review. Applied Mechanics Reviews 65, 010802.
- Klarbring, A., 1991. Derivation of a model of adhesively bonded joints by the asymptotic expansion method. International Journal of Engineering Science 29, 493–512.
- Klarbring, A., Movchan, A., 1998. Asymptotic modelling of adhesive joints. Mechanics of materials 28, 137–145.
- Kushch, V.I., 2021a. Elastic equilibrium of spherical particle composites with transversely isotropic interphase and incoherent material interface. International Journal of Solids and Structures 232, 111180.
- Kushch, V.I., 2021b. Representative unit cell model of elastic spherical particle composite with interphase and/or general imperfect interface. Mechanics of Materials 158, 103869.
- Kushch, V.I., Mogilevskaya, S.G., 2021. Anisotropic imperfect interface in elastic particulate composite with initial stress. Mathematics and Mechanics of Solids doi:10.1177/10812865211046650.
- Lebon, F., Rizzoni, R., 2011. Asymptotic behavior of a hard thin linear elastic interphase: An energy approach. International Journal of Solids and Structures 48, 441–449.
- Lebon, F., Rizzoni, R., 2018. Higher order interfacial effects for elastic waves in one dimensional phononic crystals via the Lagrange-Hamilton's principle. European Journal of Mechanics-A/Solids 67, 58–70.
- Mishuris, G., 2004. Imperfect transmission conditions for a thin weakly compressible interface. 2D problems. Archives of Mechanics 56, 103–115.
- Mogilevskaya, S., Crouch, S.L., 2002. A Galerkin boundary integral method for multiple circular elastic inclusions with homogeneously imperfect interfaces. International Journal of Solids and Structures 39, 4723–4746.
- Mogilevskaya, S., Crouch, S.L., 2004. A Galerkin boundary integral method for multiple circular elastic inclusions with uniform interphase layers. International Journal of Solids and Structures 41, 1285–1311.
- Mogilevskaya, S.G., Crouch, S.L., Stolarski, H.K., 2008. Multiple interacting circular nano-inhomogeneities with surface/interface effects. Journal of the Mechanics and Physics of Solids 56, 2298–2327.
- Mogilevskaya, S.G., Kushch, V.I., Zemlyanova, A.Y., 2019. Displacements representations for the problems with spherical and circular material surfaces. The Quarterly Journal of Mechanics and Applied Mathematics 72, 449–471.
- Mogilevskaya, S.G., Zemlyanova, A.Y., Zammarchi, M., 2018. On the elastic far-field response of a two-dimensional coated circular inhomogeneity: Analysis and applications. International Journal of Solids and Structures 130, 199–210.
- Muskhelishvili, N., 1963. Some basic problems of the mathematical theory of elasticity. Noordhoff, Groningen.
- Rizzoni, R., Dumont, S., Lebon, F., Sacco, E., 2014. Higher order model for soft and hard elastic interfaces. International Journal of Solids and Structures 51, 4137–4148.
- Rizzoni, R., Lebon, F., 2013. Imperfect interfaces as asymptotic models of thin curved elastic adhesive interphases. Mechanics Research Communications 51, 39–50.

- Ru, C., 1999. A new method for an inhomogeneity with stepwise graded interphase under thermomechanical loadings. Journal of elasticity 56, 107–127.
- Rubin, M., Benveniste, Y., 2004. A Cosserat shell model for interphases in elastic media. Journal of the Mechanics and Physics of Solids 52, 1023–1052.
- Saeb, S., Firooz, S., Steinmann, P., Javili, A., 2021. Generalized interfaces via weighted averages for application to graded interphases at large deformations. Journal of the Mechanics and Physics of Solids 149, 104234.
- Schmidt, P., 2008. Modelling of adhesively bonded joints by an asymptotic method. International journal of engineering science 46, 1291–1324.
- Serpilli, M., Dumont, S., Rizzoni, R., Lebon, F., 2021. Interface models in coupled thermoelasticity. Technologies 9, 17.
- Shabat, B.V., 1976. Introduction to complex analysis: Functions of single variable [in Russian]. Nauka, Moscow.
- Sudak, L., Mioduchowski, A., 2002. A three-phase circular inhomogeneity with imperfect interface under thermomechanical loadings in plane elasticity. Acta mechanica 158, 43–56.
- Xu, Y., He, Q.C., Gu, S.T., 2016. Effective elastic moduli of fiber-reinforced composites with interfacial displacement and stress jumps. International Journal of Solids and Structures 80, 146–157.
- Zemlyanova, A.Y., Mogilevskaya, S.G., 2018. Circular inhomogeneity with Steigmann–Ogden interface: Local fields, neutrality, and Maxwell's type approximation formula. International Journal of Solids and Structures 135, 85–98.
- Zhu, Q.Z., Gu, S.T., Yvonnet, J., Shao, J.F., He, Q.C., 2011. Three-dimensional numerical modelling by XFEM of spring-layer imperfect curved interfaces with applications to linearly elastic composite materials. International Journal for Numerical Methods in Engineering 88, 307–328.